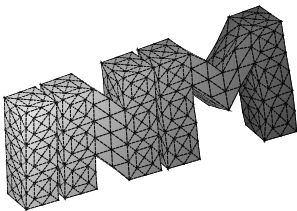


---

*hp*-Finite Element Simulation of Three-Dimensional  
Eddy Current Problems  
on Multiply Connected Domains

P.D. Ledger, S. Zaglmayr

---



**Berichte aus dem  
Institut für Numerische Mathematik**



**Technische Universität Graz**

---

*hp*-Finite Element Simulation of Three-Dimensional  
Eddy Current Problems  
on Multiply Connected Domains

P.D. Ledger, S. Zaglmayr

---

**Berichte aus dem  
Institut für Numerische Mathematik**

Bericht 2010/02

Technische Universität Graz  
Institut für Numerische Mathematik  
Steyrergasse 30  
A 8010 Graz

**WWW:** <http://www.numerik.math.tu-graz.at>

© Alle Rechte vorbehalten. Nachdruck nur mit Genehmigung des Autors.

# *hp*-Finite Element Simulation of Three-Dimensional Eddy Current Problems on Multiply Connected Domains

P.D. Ledger<sup>#</sup>, S. Zaglmayr<sup>\*</sup>

<sup>#</sup> Civil and Computational Engineering Research Centre, School of Engineering,  
Swansea University, United Kingdom.

P.D.Ledger@swansea.ac.uk

<sup>\*</sup> Institute for Computational Mathematics, Graz University of Technology, Austria.

Sabine.Zaglmayr@tugraz.at

**Abstract** This work considers the accurate and efficient finite element simulation of three-dimensional eddy current problems. We review the application of  $\mathbf{H}$  and  $\mathbf{A}$  based formulations for multiply connected domains for the cases where the conductor has a handle and/or a hole. We focus on an hierarchical *hp*-finite element discretization of the  $\mathbf{A}$  based formulation that is gauged by regularization. Based on an explicit kernel splitting of the underlying *hp*-finite element basis, we present a novel preconditioning technique for eddy current problems. We demonstrate its validity on multiply connected domains and include a series of numerical examples to show the effectiveness of the proposed approach.

*Keywords* eddy current problems, multiply connected domains, *hp*-finite elements , efficient preconditioning

# 1 Introduction

The governing equations for the eddy current model [19], in a time-harmonic setting, are

$$\operatorname{curl} \mathbf{E} = -i\omega\mu\mathbf{H}, \quad (1a)$$

$$\operatorname{curl} \mathbf{H} = \sigma\mathbf{E} + \mathbf{J}^S, \quad (1b)$$

$$\nabla \cdot \mathbf{D} = \rho_V, \quad (1c)$$

$$\nabla \cdot \mathbf{B} = 0, \quad (1d)$$

where  $\mathbf{E}$ ,  $\mathbf{H}$ ,  $\mathbf{D}$  and  $\mathbf{B}$  are the electric, magnetic, electric displacement and magnetic displacement fields, respectively. The term  $\mathbf{J}^S$  represents external current sources, which are assumed to be divergence free. The complex imaginary unit is  $i = \sqrt{-1}$ . The quantities  $\omega$ ,  $\epsilon$ ,  $\mu$ ,  $\sigma$  and  $\rho_V$  are the (angular) frequency, permittivity, permeability, conductivity and volume charge density, respectively. As standard  $\mu_r = \mu/\mu_0$  is the relative permeability,  $\mu_0 = 4\pi 10^{-7} \text{Hm}^{-1}$  is the permeability of free space,  $\epsilon_r = \epsilon/\epsilon_0$  is the relative permittivity and  $\epsilon_0 = 8.85 \times 10^{-12} \text{F/m}$  is the permittivity of free space. The electric and magnetic fields are linked to the electric and magnetic displacement fields by the constitutive relationships

$$\mathbf{D} = \epsilon\mathbf{E}, \quad \mathbf{B} = \mu\mathbf{H}. \quad (2)$$

Equations (1a)-(1d) represent a quasi-static approximation of the time harmonic Maxwell equations and are easily obtained if one assumes that the displacement currents in Ampere's law are negligible and one substitutes Ohm's law,  $\mathbf{J} = \sigma\mathbf{E} + \mathbf{J}^S$ , for the volume current density,  $\mathbf{J}$ . For a given length scale  $L$ , this model reduction is an acceptable approach if either

$$\sqrt{\epsilon\mu}L\omega \ll 1, \quad \text{or} \quad \epsilon\omega/\sigma \ll 1,$$

holds, see eg [19, 5, 36] for a justification. For the problems under consideration in this work, the ratio  $\epsilon\omega/\sigma$  is of the order of  $10^{-16}$  and so the eddy current model represents a very acceptable approximation. The problem set-up considered here comprises of a conducting region  $\Omega_C$ , where  $\sigma(x) \geq \sigma_0 > 0$ , which is surrounded by an infinite non conducting region  $\Omega_N^\infty$ , where  $\sigma = 0$ . Furthermore, we initially assume a trivial topology, such that the conductor has no handles or cavities (holes) and a given divergence-free source  $\mathbf{J}^S$  in the non-conducting domain. The situation is illustrated in Figure 1. Later, we shall consider what happens when the assumptions about the topology are relaxed.

On neglecting the displacement current, the eddy current problem reduces to a magnetostatic problem in  $\Omega_N^\infty$  and we claim the magnetic and electric field to decay at infinity as

$$\lim_{|\mathbf{x}| \rightarrow \infty} \mathbf{H}(\mathbf{x}) = \mathcal{O}\left(\frac{1}{|\mathbf{x}|^2}\right), \quad \lim_{|\mathbf{x}| \rightarrow \infty} \mathbf{E}(\mathbf{x}) = \mathcal{O}\left(\frac{1}{|\mathbf{x}|^2}\right).$$

Numerically, the unbounded region can be handled in a number of different ways, for instance by the coupling of finite and boundary elements eg [56, 37, 16, 55, 38, 75, 14, 44, 45, 21, 79, 74, 19]. A number of other alternatives are also described by Bossavit [19] (Chapter 7). However, for simplicity, we assume that  $\Omega_N^\infty$  is truncated a finite distance from the conductor by a bounding box  $M$ , denote the truncated non conducting region by  $\Omega_N = \Omega_N^\infty \cap M$ , and impose an appropriate boundary condition on  $\partial M$ .

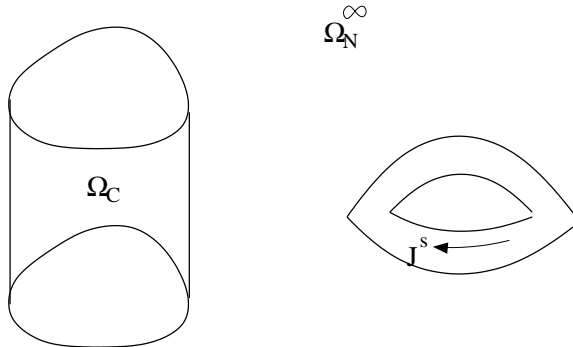


Figure 1: Illustration of an eddy current problem of a solid conductor  $\Omega_C$  surrounded by an infinite non-conducting region  $\Omega_N^\infty$  and excited by a coil with current  $J^s$

There are a number of possible formulations of the quasi-stationary Maxwell equations (1a)-(1d) in terms of primal variables or auxiliary vector or scalar potentials as well as hybrid formulations. A review of several variants can be found in Biro [13], and in earlier works eg Biro and Preis [15]. Hiptmair and Sterz [36] have investigated different excitation possibilities for eddy current problems expressed in terms of primal and potential variables. There is also considerable discussion concerning the application of these different formulations to multiply connected domains, for example [19, 36, 31, 16, 62].

In this work we pick out the following two variants: First, a formulation which describes (1a)-(1d) only in terms of the magnetic field, namely the  $\mathbf{H}$  based formulation, and, secondly, the  $\mathbf{A}$  based formulation relying on the introduction of an auxiliary magnetic vector potential  $\mathbf{A}$ . Depending on the problem under consideration and its topological properties, and the formulation adopted, one sometimes also makes use of scalar magnetic potentials  $\psi$  and scalar electric potentials  $\Phi$ . For these different eddy current formulations, the vector valued fields  $\mathbf{H}$  and  $\mathbf{A}$  are conformingly discretized with tangential continuous finite elements, which were first proposed by Nédélec [57, 58]. The lowest order Nédélec elements of the first kind are commonly known as edge elements as there is a single degree of freedom associated with each edge. The scalar electric or magnetic potentials lie in  $H^1(\Omega)$  and hence are discretized by standard continuous finite elements. The corresponding lowest  $H^1$  approximation consists of the standard nodal hat functions associated with the vertices of the elements. A general overview of finite element methods for Maxwell's equations can be found, for example, in the book by Monk [54].

Higher order finite elements, in particular  $hp$ -finite elements, offer superior approximation properties as it is known that using the correct combination of mesh subdivision ( $h$ -refinement) and polynomial enrichment ( $p$ -refinement) leads to exponential convergence of the finite element solution for problems with smooth solutions as well as piecewise analytic solutions with singularities due to re-entrant corners and edges [4, 68, 66, 24, 25]. Crucial to the efficient implementation of the  $hp$ -finite element method are hierarchic sets of basis functions for higher order Nédélec and continuous elements. Several variants of these basis functions have been proposed including, Webb and Forghani [76], Webb [73], Demkowicz *et al.* [27, 59], Ainsworth and Coyle [1, 2], Bossavit [20] and Schöberl and Zaglmayr [65]. In the context of computational electromagnetism, these elements have been applied to a range of applications including eigenvalue computation [35, 3, 23] and electromagnetic scat-

tering [28, 26, 22, 52, 46, 51, 49, 50, 53] where evidence of accurate solutions and exponential convergence, for the correct combination of  $h$  and  $p$  refinements, has been demonstrated.

In order to apply  $hp$ -finite elements to practical problems an efficient means of solving the linear system is required. Efficient solution techniques for eddy current problems include multigrid preconditioning approaches developed by Hiptmair [32], Arnold *et al.* [9], Reitzinger and Schöberl [60], Becket *et al.* [12] and Bachinger *et al.* [11] as well as related work on preconditioning similar systems eg [6]. Nevertheless, these methods are mainly designed, and applied, to finite element discretizations with fixed or low polynomial degrees. The hierarchic basis functions proposed by Schöberl and Zaglmayr lend themselves to a parameter-robust iterative two-level solver: Assuming that an appropriate  $h$ -version solver on the low-order space (the coarse level) is available, simple block Jacobi smoothing is sufficient on the high-order level (the fine level). This preconditioning technique is described and analysed in [65, 78] and has been modified for wave propagation problems by Ledger [48, 47]. In this work, we combine and extend these strategies by further exploiting the discrete space splitting of the underlying hierarchical  $hp$ -finite element basis and suggest an improved version of a hierarchical  $hp$ -finite element solver for eddy current problems.

The paper proceeds as follows: The first part describes several different variational formulations that are commonly used for solving the eddy current problem. In particular, the  $\mathbf{H}$  based and the  $\mathbf{A}$  based formulations will be discussed in detail for simply connected domains in Section 2. In Section 3 the appropriate treatment of eddy current problems on multiply connected domains will be discussed and the necessary modifications to the  $\mathbf{H}$  based and the  $\mathbf{A}$  based formulations will be outlined when handles and cavities (holes) are present in the domain. The relative merits of the  $\mathbf{H}$  based and  $\mathbf{A}$  based formulations are discussed in Section 4. In the second part of the paper, an  $hp$ -finite element approach to the solution of the  $\mathbf{A}$  based formulation of the eddy current solution on multiply connected domains will be introduced. An improved preconditioner is introduced as a novel contribution, which allows the rapid solution of the linear equation and consequently the efficient solution of these problems. Section 5 describes the choice of  $hp$ -finite element basis functions as introduced in [65, 78] and Section 6 describes an efficient preconditioning technique for this finite element basis. Numerical results are presented in Section 7, which show the application of these techniques to eddy current problems set on simply connected and multiply connected domains.

## 2 Variational approaches to the solution of eddy current problems

We first introduce some notation and review some basic results on the function spaces employed in this work.

### 2.1 Basic assumption and notations

In the sequel reference will be made to the following definitions: Let  $\Omega = \text{interior}(\overline{\Omega}_N \cup \overline{\Omega}_C)$ ,  $\Omega_N, \Omega_C \subset \mathbb{R}^3$  be bounded, open Lipschitz-domains with  $\Omega_C \cap \Omega_N = \emptyset$ . We refer to the unit outward normal vector on boundaries by  $\mathbf{n}$ . In this section we assume the conducting domain  $\Omega_C$  as well as  $\Omega$  to be contractible (simply connected with connected boundary [19]). This assumption will be weakened in Section 3.

Furthermore, we introduce the following notation: Let  $[[\mathbf{u} \times \mathbf{n}]] := \mathbf{u}|_{\Omega_1} \times \mathbf{n}_1 + \mathbf{u}|_{\Omega_2} \times \mathbf{n}_2$



denote the jump of the tangential component of a vector quantity  $\mathbf{u}$  over some interface  $\Gamma = \partial\Omega_1 \cap \partial\Omega_2$  between two disjoint regions  $\Omega_1$  and  $\Omega_2$ . Here,  $\mathbf{n}_1$  denotes the outer normal vector on  $\partial\Omega_1$  and  $\mathbf{n}_2 = -\mathbf{n}_1$  the outer normal vector of  $\partial\Omega_2$ . We use the analogous notation for the jump in the normal component, namely  $[[\mathbf{u} \cdot \mathbf{n}]] := \mathbf{u}|_{\Omega_1} \cdot \mathbf{n}_1 + \mathbf{u}|_{\Omega_2} \cdot \mathbf{n}_2$ .

In the variational framework we refer to the  $L_2(\Omega)$ -inner product by  $(\mathbf{u}, \mathbf{v})_\Omega := \int_\Omega \mathbf{u}(x) \cdot \mathbf{v}(x) dx$ .

## 2.2 Function spaces and mapping properties of differential operators

In view of a variational formulation of Maxwell's equations, we introduce the following scalar and vector-valued function spaces:

$$\begin{aligned} H^1(\Omega) &:= \{v \in L_2(\Omega) : \nabla v \in (L_2(\Omega))^3\}, \\ H(\text{curl}, \Omega) &:= \{\mathbf{u} \in (L_2(\Omega))^3 : \text{curl } \mathbf{u} \in (L_2(\Omega))^3\}, \\ H(\text{div}, \Omega) &:= \{\mathbf{u} \in (L_2(\Omega))^3 : \text{div } \mathbf{u} \in L_2(\Omega)\}. \end{aligned}$$

The de Rham sequence

$$\mathbb{R} \xrightarrow{id} H^1(\Omega) \xrightarrow{\nabla} H(\text{curl}, \Omega) \xrightarrow{\text{curl}} H(\text{div}, \Omega) \xrightarrow{\text{div}} L_2(\Omega) \quad (3)$$

is fundamental in the functional as well as in the numerical analysis of Maxwell's equations [19, 57, 8, 33, 30, 25, 54]. It summarises the relation between the above function spaces and the mapping properties of their natural differential operators. For contractible domains the de Rham sequence (3) is exact [19, 8], namely

$$\begin{aligned} \mathbb{R} &= \{v \in H^1(\Omega) : \nabla v = 0\}, \\ \nabla H^1(\Omega) &= \{\mathbf{v} \in H(\text{curl}, \Omega) : \text{curl } \mathbf{v} = 0\}, \\ \text{curl } H(\text{curl}, \Omega) &= \{\mathbf{v} \in H(\text{div}, \Omega) : \text{div } \mathbf{v} = 0\}, \\ \text{div } H(\text{div}, \Omega) &= L_2(\Omega). \end{aligned}$$

The range of a differential operator in the sequence is not only a subset but really coincides with the nullspace of the succeeding differential operator. Finally, the divergence operator is surjective.

**Remark 2.1.** *Analogous de Rham sequences can be formulated for function spaces obeying boundary conditions, see eg [33, 54]. Considering the subspaces of functions having zero canonical trace*

$$\begin{aligned} H_0^1(\Omega) &:= \{v \in H^1(\Omega) : v = 0 \text{ on } \partial\Omega\}, \\ H_0(\text{curl}, \Omega) &:= \{\mathbf{u} \in H(\text{curl}, \Omega) : \mathbf{n} \times \mathbf{u} = 0 \text{ on } \partial\Omega\}, \end{aligned}$$

*the null space of the curl operator (for a topologically trivial domain  $\Omega$ ) is*

$$\nabla H_0^1(\Omega) = \{\mathbf{v} \in H_0(\text{curl}, \Omega) : \text{curl } \mathbf{v} = 0\}.$$

### 2.3 Variational formulation of the $\mathbf{H}$ based formulation

One suitable formulation for solving eddy current problems is the  $\mathbf{H}$  based formulation, which can be traced back to the early work by Bossavit and V erit e [21]. The  $\mathbf{H}$  based formulation is best expressed as

$$\operatorname{curl} \mathbf{E} = i\omega\mu\mathbf{H} \quad \text{in } \Omega, \quad (4a)$$

$$\operatorname{curl} \mathbf{H} = \sigma\mathbf{E} + \mathbf{J}^s \quad \text{in } \Omega_C, \quad (4b)$$

$$\operatorname{curl} \mathbf{H} = \mathbf{J}^s \quad \text{in } \Omega_N, \quad (4c)$$

with boundary and interface conditions

$$\mathbf{n} \times \mathbf{H} = 0 \quad \text{on } \partial\Omega, \quad (4d)$$

$$[[\mathbf{n} \times \mathbf{H}]] = 0 \quad \text{on } \partial\Omega_N \cap \partial\Omega_C, \quad (4e)$$

$$[[\mathbf{n} \times \mathbf{E}]] = 0 \quad \text{on } \partial\Omega_N \cap \partial\Omega_C. \quad (4f)$$

**Remark 2.2.** For simplicity, we truncate  $\Omega_N^\infty$  by imposing  $\mathbf{n} \times \mathbf{H} = 0$  on the truncated boundary  $\partial\Omega$  with  $\Omega_N \neq \emptyset$ . In the paper of Bossavit and V erit e [21] an alternative approach to the truncation  $\Omega_N$ , which allows  $\partial\Omega$  to be brought close to, or if  $\operatorname{supp}\mathbf{J}^s \subset \Omega_C$ , on the surface of the conductor  $\partial\Omega_C$  itself, is employed.

Following Hiptmair and Sterz [36] we define

$$\mathcal{V}(\mathbf{J}^s) = \{\mathbf{v} \in H(\operatorname{curl}, \Omega), \operatorname{curl} \mathbf{v} = \mathbf{J}^s \text{ in } \Omega_N, \mathbf{n} \times \mathbf{v} = 0 \text{ on } \partial\Omega\},$$

the weak form of this problem can then be written as: Find  $\mathbf{H} \in \mathcal{V}(\mathbf{J}^s)$  such that

$$(\sigma^{-1} \operatorname{curl} \mathbf{H}, \operatorname{curl} \mathbf{v})_{\Omega_C} + i\omega(\mu\mathbf{H}, \mathbf{v})_\Omega = (\sigma^{-1} \operatorname{curl} \mathbf{J}^s, \mathbf{v})_{\Omega_C} \quad \forall \mathbf{v} \in \mathcal{V}(\mathbf{0}). \quad (5)$$

In the case of current excitation, with  $\operatorname{supp}\mathbf{J}^s \subset \Omega_N$ , one chooses a field  $\mathbf{H}^s \in H(\operatorname{curl}, \Omega)$  such that  $\operatorname{curl} \mathbf{H}^s = \mathbf{J}^s$  in  $\Omega_N$  and the weak form becomes: Find  $\mathbf{H} = \mathbf{H}^s + \mathbf{H}'$  with  $\mathbf{H}' \in \mathcal{V}(\mathbf{0})$  such that

$$(\sigma^{-1} \operatorname{curl} \mathbf{H}, \operatorname{curl} \mathbf{v})_{\Omega_C} + i\omega(\mu\mathbf{H}, \mathbf{v})_\Omega = 0 \quad \forall \mathbf{v} \in \mathcal{V}(\mathbf{0}). \quad (6)$$

Note that in the topologically trivial case, which is precisely the case shown in Figure 1,  $\mathbf{H}'$  can be written in the simple form  $\mathbf{H}' = -\nabla\psi'$  in  $\Omega_N$ , where  $\psi' \in H_0^1(\Omega_N)$  is a scalar potential. Other types of excitation are discussed by Hiptmair and Sterz [36]. Note that this formulation is also often referred to in the literature as the  $\mathbf{H} - \psi^1$  formulation (eg [79]).

### 2.4 Variational formulation of the $\mathbf{A}$ based formulation and gauging conditions

A second possible formulation for solving the eddy current problem is the  $\mathbf{A}$  based formulation. This formulation is based on fulfilling (1d) exactly by introducing a vector potential  $\mathbf{A}$ , which is such that  $\mathbf{B} = \operatorname{curl} \mathbf{A}$ . This vector potential is not unique. In the conducting region  $\Omega_C$

---

<sup>1</sup>We adopt the convention that the variables used in  $\Omega_C$  are listed first and those used in  $\Omega_N$  are listed second.

we uniquely define the vector potential by *temporal gauging* such that  $\mathbf{E} = -i\omega\mathbf{A}$ . Following Hiptmair and Sterz [36] we denote this as the  $\mathbf{A}$  based formulation:

$$\operatorname{curl} \mu^{-1} \operatorname{curl} \mathbf{A} + i\omega\sigma\mathbf{A} = 0 \quad \text{in } \Omega_C, \quad (7a)$$

$$\operatorname{curl} \mu^{-1} \operatorname{curl} \mathbf{A} = \mathbf{J}^s \quad \text{in } \Omega_N, \quad (7b)$$

with boundary and transmission conditions

$$\mathbf{n} \times \mathbf{A} = 0 \quad \text{on } \partial\Omega, \quad (7c)$$

$$[[\mathbf{n} \times \mathbf{A}]] = 0 \quad \text{on } \partial\Omega_N \cap \partial\Omega_C, \quad (7d)$$

$$[[\mathbf{n} \times \mu^{-1} \operatorname{curl} \mathbf{A}]] = 0 \quad \text{on } \partial\Omega_N \cap \partial\Omega_C. \quad (7e)$$

Note that this is often referred to as the  $\mathbf{A}^* - \mathbf{A}$  formulation (eg [13]), which indicates that the modified vector potential,  $\mathbf{A}^*$ , is used in  $\Omega_C$  and the vector potential  $\mathbf{A}$  is used in  $\Omega_N$ <sup>2</sup>. We remark that in the non-conducting domain,  $\Omega_N$ , the above formulation is still ungauged and that  $\mathbf{A}$  is defined up to gradients  $\nabla H_0^1(\Omega_N)$ . As previously mentioned, there are several ways to account the restriction to a bounded domain  $\Omega$ , here we claim that (7c) implies  $\mathbf{n} \times \mathbf{E} = 0$  on the outer boundary  $\partial\Omega$ .

We introduce a parameter  $\kappa$  that is such that  $\kappa = 0$  in the non-conducting domain  $\Omega_N$  and  $\kappa = i\mu_0\omega\sigma$  in the conducting domain  $\Omega_C$ . The weak formulation of (7) then reads as follows: Find  $\mathbf{A} \in H_0(\operatorname{curl}, \Omega)$  such that

$$(\mu_r^{-1} \operatorname{curl} \mathbf{A}, \operatorname{curl} \mathbf{v})_\Omega + (\kappa\mathbf{A}, \mathbf{v})_{\Omega_C} = (\mu_0\mathbf{J}^s, \mathbf{v})_{\Omega_N} \quad \forall \mathbf{v} \in H_0(\operatorname{curl}, \Omega). \quad (8)$$

#### 2.4.1 Gauging strategies in $\Omega_N$

Due to vanishing  $\kappa$  in the non-conducting domain  $\Omega_N$  the solution  $\mathbf{A} \in H_0(\operatorname{curl}, \Omega)$  is unique only up to gradient functions in  $\Omega_N$ . There are various ways to enforce uniqueness, which include working with factor spaces or by introducing further constraints on the solution. One commonly used choice is the *Coulomb gauge*

$$\operatorname{div} \mathbf{A} = 0 \text{ in } \Omega_N. \quad (9)$$

In a weak sense the Coulomb gauge is equivalent to  $\mathbf{A}$  being orthogonal to all gradients  $\nabla H_0^1(\Omega_N)$  (continuously extended by zero onto  $\Omega$ ). This leads to a mixed problem of the form: Find  $\mathbf{A} \in H_0(\operatorname{curl}, \Omega)$  and  $\Phi \in H_0^1(\Omega)$  such that

$$(\mu_r^{-1} \operatorname{curl} \mathbf{A}, \operatorname{curl} \mathbf{v})_\Omega + (\kappa\mathbf{A}, \mathbf{v})_\Omega + (\nabla\Phi, \mathbf{v})_{\Omega_N} = (\mu_0\mathbf{J}^s, \mathbf{v})_{\Omega_N}, \quad (10a)$$

$$(\nabla\Psi, \mathbf{A})_{\Omega_N} = 0, \quad (10b)$$

for all  $\mathbf{v} \in H(\operatorname{curl}, \Omega)$  and for all  $\Psi \in H_0^1(\Omega_N)$ , where  $\Phi$  is a Lagrange multiplier, which has been introduced in order to enforce the Coulomb gauge in weak sense.

As an alternative, and following [10, 65, 78], we introduce the primal perturbed problem: Let  $\varepsilon > 0$  be a small perturbation parameter, then: Find  $\mathbf{A}^\varepsilon \in H_0(\operatorname{curl}, \Omega)$  such that

$$(\mu_r^{-1} \operatorname{curl} \mathbf{A}^\varepsilon, \operatorname{curl} \mathbf{v})_\Omega + (\kappa\mathbf{A}^\varepsilon, \mathbf{v})_{\Omega_C} + (\varepsilon\mathbf{A}^\varepsilon, \mathbf{v})_{\Omega_N} = (\mu_0\mathbf{J}^s, \mathbf{v})_{\Omega_N} \quad \forall \mathbf{v} \in H_0(\operatorname{curl}, \Omega). \quad (11)$$

---

<sup>2</sup>In this work we choose not to make a distinction between  $\mathbf{A}^*$  and  $\mathbf{A}$ .

The analysis of [11, 78] for the perturbed version of the magnetostatic regime carries over to the perturbed eddy current problem (11): The unique solution  $\mathbf{A}^\varepsilon$  of the perturbed problem lies in  $H_0(\text{curl}, \Omega) \cap (\nabla H_0^1(\Omega_N))^\perp$ . There holds  $\|\mathbf{A} - \mathbf{A}^\varepsilon\|_{H(\text{curl}, \Omega)} \leq c \cdot \varepsilon \|\mathbf{J}^s\|_{H(\text{curl}, \Omega)^*}$  where the constant  $c$  is independent of  $\varepsilon$  and  $\mathbf{A}$  denotes the solution of the mixed problem (10).

**Remark 2.3.** *The perturbation parameter  $\varepsilon$  is chosen as  $0 < \varepsilon \ll |\kappa|$ . Hence, for a stable numerical discretization the solver has to be robust as  $\varepsilon \rightarrow 0$  (see Section 6 and [65, 9, 32, 78, 60]).*

In view of a compact notation we introduce a perturbed parameter  $\tilde{\kappa} := \begin{cases} \varepsilon & \text{in } \Omega_N \\ \kappa & \text{in } \Omega_C \end{cases}$ . The weak problem then reads: Find  $\mathbf{A}^\varepsilon \in H_0(\text{curl}, \Omega)$  such that

$$(\mu_r^{-1} \text{curl } \mathbf{A}^\varepsilon, \text{curl } \mathbf{v})_\Omega + (\tilde{\kappa} \mathbf{A}^\varepsilon, \mathbf{v})_\Omega = (\mu_0 \mathbf{J}^s, \mathbf{v})_{\Omega_N} \quad \forall \mathbf{v} \in H_0(\text{curl}, \Omega). \quad (12)$$

**Remark 2.4.** *In Section 5.2 we introduce an alternative gauging strategy of (8), which enables a reduced hp-finite element discretization to be realised.*

### 3 Multiply connected domains

In this section we wish to give a concise review of the way in which the  $\mathbf{H}$  based and  $\mathbf{A}$  based formulations can be applied to problems with multiply connected domains. Specifically, we consider conductors,  $\Omega_C$ , that have either a handle or a cavity (hole), which are excited by divergence-free current sources in the form of coils located in  $\Omega_N$ . Our review draws on the existing literature [21, 55, 79, 74, 77, 16, 37, 19, 36, 62], which considers the application of different formulations of the eddy current problems to multiply connected domains.

In the case of general Lipschitz domains the classical de Rham sequence (3) is no longer an exact sequence. The range of a differential operator in the sequence (3) is still a subspace of the null space of the preceding operator, but the spaces no longer coincide [19, 8, 7]. In such cases finite dimensional cohomology spaces must be added to regain exactness. The dimension of these spaces depend on the topological properties of the domain in consideration,  $\Omega$ , precisely on its Betti numbers.

The zeroth Betti number,  $\beta_0(\Omega)$ , is the number of connected parts of  $\Omega$ , which for a bounded connected region in  $\mathbb{R}^3$  is always 1. The first Betti number,  $\beta_1(\Omega)$  is the genus, i.e. the number of handles of  $\Omega$ , while the second Betti number,  $\beta_2(\Omega)$  is one less than the number of connected parts of the boundary  $\partial\Omega$ , i.e. the number of holes.

In particular, in the situation where  $\Omega$  contains  $\beta_1(\Omega)$  handles, a non-bounding orientated path, known as a loop can be associated with each handle. For  $\beta_1(\Omega)$  loops, one can also construct  $\beta_1(\Omega)$  cuts of  $\Omega$  that can be represented by piece wise orientated surfaces, known as Seifert surfaces. If  $\Sigma_1, \dots, \Sigma_N$ , where  $N := \beta_1(\Omega)$ , stands for the complete set of cuts, then every curl free vector field in  $\Omega \setminus (\Sigma_1 \cup \dots \cup \Sigma_N)$  can be expressed as the gradient of a scalar field. However, if one considers a curl free vector field in all of  $\Omega$  it need not be a gradient but instead there exists a finite dimensional cohomology space  $\mathcal{H}^1(\Omega) \subset H(\text{curl}, \Omega)$  with  $\dim \mathcal{H}^1(\Omega) = \beta_1(\Omega)$  such that

$$\{\mathbf{u} \in H(\text{curl}, \Omega), \text{curl } \mathbf{u} = 0\} = \nabla H^1(\Omega) \oplus \mathcal{H}^1(\Omega) \quad (13)$$

In a similar way if  $\beta_2(\Omega) \neq 0$  this would indicate that there are divergence free fields in  $\Omega$  that are not expressed as the curl of some vector field. For further details we refer to

[41, 42, 19, 62, 34, 36, 31] and references therein.

To illustrate the importance of this we consider a number of selected concrete examples.

### 3.1 A conductor with a handle

The concept of a handle is best realised by considering the image of a coffee cup. Clearly, conductors are rarely of this shape, but, topologically speaking, this is the same as a torus or a conducting plate with a hole piecing through it. The conductor plate shown in Figure 2 is often referred to as a *conducting plate with a hole* eg [29], however, to avoid confusion with our second example we shall refer to it as a conducting plate with a handle. For this example,  $\beta_0(\Omega_C) = \beta_0(\Omega_N) = 1$ ,  $\beta_1(\Omega_C) = \beta_1(\Omega_N) = 1$  and  $\beta_2(\Omega_C) = \beta_2(\Omega_N) = 0$ .

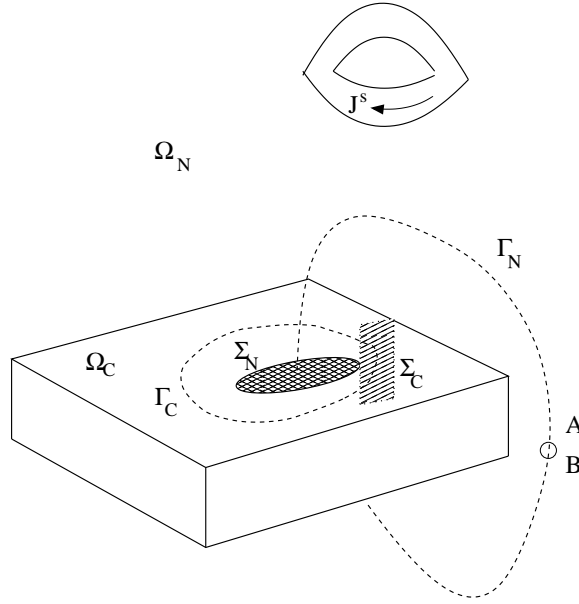


Figure 2: Illustration of an eddy current problem of a conductor  $\Omega_C$  with a handle surrounded by a non-conducting region  $\Omega_N$  and current excitation  $\mathbf{J}^s$  by a coil (note that  $\partial\Omega$  is not shown)

We first examine the application of the  $\mathbf{H}$  based formulation to this problem, making the naive (and ultimately incorrect) choice that  $\mathbf{H}' = -\nabla\psi'$  in  $\Omega_N$ . The validity of the approach can be investigated by considering the contour integral of  $\mathbf{H} \cdot \boldsymbol{\tau}$  along the loop  $\Gamma_N$  yielding

$$\begin{aligned} \oint_{\Gamma_N} \mathbf{H} \cdot \boldsymbol{\tau} dl &= \oint_{\Gamma_N} (\mathbf{H}^s - \nabla\psi') \cdot \boldsymbol{\tau} dl = \oint_{\Gamma_N} \mathbf{H}^s \cdot \boldsymbol{\tau} dl - \oint_{\Gamma_N} \nabla\psi' \cdot \boldsymbol{\tau} dl = \\ &= \int_{S_N} \text{curl } \mathbf{H}^s \cdot \mathbf{n} ds - (\psi^B - \psi^A) = \int_{S_N} \mathbf{J}^s \cdot \mathbf{n} ds, \end{aligned} \quad (14)$$

where the contour integral of the tangential component of  $\mathbf{H}^s$  is converted to a surface integral with the help of Stokes theorem. The surface  $S_N$  is the surface that is enclosed by the contour  $\Gamma_N$ . The relation  $\psi^B = \psi^A$  follows since the location of  $B$  is the same as  $A$  and the value

of  $\psi'$  at these points must be the same for a single-valued potential. On the other hand, considering an integral of the normal component of  $\text{curl } \mathbf{H}$  on the surface  $S_N$  yields

$$\int_{S_N} \text{curl } \mathbf{H} \cdot \mathbf{n} ds = \int_{S_N} (\mathbf{J}^s + \mathbf{J}^e) \cdot \mathbf{n} ds, \quad (15)$$

where  $\mathbf{J}^e = \sigma \mathbf{E}$  is the eddy current in the conductor. Consequently, making the choice  $\mathbf{H} = -\nabla \psi'$  in  $\Omega_N$  is unable to correctly predict the fields when a conductor has a handle. To overcome this, a cut,  $\Sigma_N$ , is usually introduced in the hole that has been punched through the conductor and the scalar potential  $\psi'$  is allowed to jump at this location [19]. The jump in the potential means that it is multiply valued so that the jump at the cut corresponds to

$$\psi'|_{\Sigma_N^+} - \psi'|_{\Sigma_N^-} = \int_{S_N} \mathbf{J}^e \cdot \mathbf{n} ds, \quad (16)$$

and consequently, the fields are correctly predicted. This is also what the theory predicts: since  $\beta_1(\Omega_N) = 1$  there exists a loop,  $\Gamma_N$ , and with it is associated a cutting surface,  $\Sigma_N$ . Curl free fields in all of  $\Omega_N$ , that are not gradients of a scalar field, can be represented by a finite dimensional cohomology space  $\mathcal{H}^1(\Omega_N) \subset H(\text{curl}, \Omega_N)$  of dimensional  $\dim \mathcal{H}^1(\Omega_N) = \beta_1(\Omega_N) = 1$ , which, in turn, is represented by the jump in  $\psi'$  at  $\Sigma_N$ <sup>3</sup>. A common misinterpretation is that the cut is introduced in order to convert a multiply connected domain into one that is simply connected eg [71], it is noteworthy that a statement along these lines led to a heated debate in the literature [18, 43]. The correct mathematical definition of a cut has been proposed by Kotigua [41], its purpose being to make every curl free field equal to the gradient of a scalar in  $\Omega$  minus the cut(s) [19]. For further details of the computational implementation see [19] and [41, 42] where an algorithm for the detecting the location of the cutting (or Siefert) surface is described.

Reconsidering the contour integral of  $\mathbf{H} \cdot \boldsymbol{\tau}$  along the loop  $\Gamma_N$ , we next consider the validity of the  $\mathbf{A}$  based formulation. A similar approach to that performed in equation (14) yields

$$\begin{aligned} \oint_{\Gamma_N} \mathbf{H} \cdot \boldsymbol{\tau} dl &= \oint_{\Gamma_N} \mu^{-1} \text{curl } \mathbf{A} \cdot \boldsymbol{\tau} dl = \int_{S_N} \text{curl } \mu^{-1} \text{curl } \mathbf{A} \cdot \mathbf{n} ds = \\ &= \int_{S_N} (\mathbf{J}^s - i\omega\sigma \mathbf{A}) \cdot \mathbf{n} ds = \int_{S_N} (\mathbf{J}^s + \mathbf{J}^e) \cdot \mathbf{n} ds, \end{aligned} \quad (17)$$

and consequently the fields are correctly predicted in this case as one does not attempt to represent curl free fields as the gradient of scalar functions.

### 3.2 A conductor with a cavity (or hole)

The concept of a cavity (or hole) is best realised by considering the illustration shown in Figure 3. In this figure a conducting plate containing an internal cavity  $\Omega_0$  is shown. Also depicted is a surface  $S_1$ , which is located in  $\Omega_N$  and that totally encloses the conductor. The region between the outer boundary of the conductor  $\partial\Omega_C \setminus \partial\Omega_C \cap \partial\Omega_0$  and the surface  $S_1$  is denoted by  $\Omega_1$ . For this example,  $\beta_0(\Omega_C) = \beta_0(\Omega_N) = 1$ ,  $\beta_1(\Omega_C) = \beta_1(\Omega_N) = 0$  and  $\beta_2(\Omega_C) = \beta_2(\Omega_N) = 1$ .

---

<sup>3</sup>In a similar manner, due to the existence of the loop,  $\Gamma_C$ , and associated surface,  $\Sigma_C$ , curl free fields in all of  $\Omega_C$ , which are not gradients of a scalar field, can be represented by a finite dimensional cohomology space  $\mathcal{H}^1(\Omega_C) \subset H(\text{curl}, \Omega_C)$  of dimensional  $\dim \mathcal{H}^1(\Omega_C) = \beta_1(\Omega_C) = 1$ .

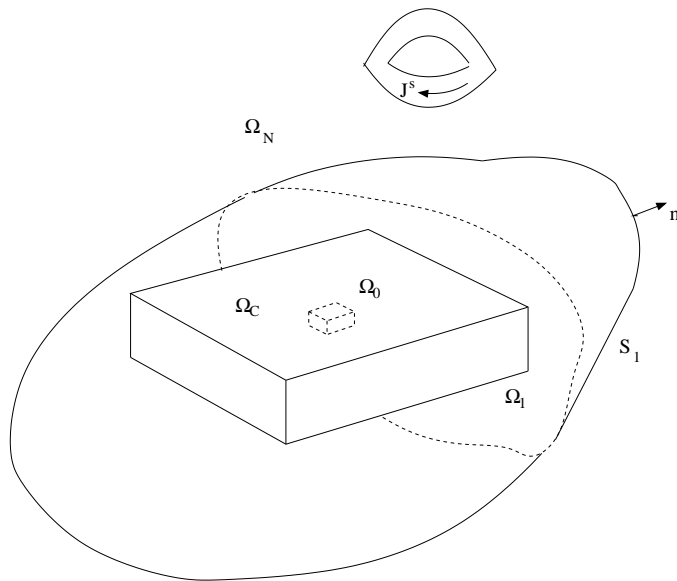


Figure 3: Illustration of an eddy current problem consisting of a conducting plate  $\Omega_C$  with a cavity  $\Omega_0$ . Also shown is an arbitrary surface  $S_1$  which totally encloses the conductor. The current excitation  $\mathbf{J}^s$  is by a coil in  $\Omega_N$  (note that  $\partial\Omega$  is not shown)

We first examine the application of the  $\mathbf{H}$  based formulation to this problem, the validity of the approach can be considered by considering the surface integral of  $\mathbf{n} \cdot \mathbf{B}$  on the surface  $S_1$

$$\int_{S_1} \mathbf{n} \cdot \mathbf{B} ds = \int_{\Omega_1 + \Omega_C + \Omega_0} \nabla \cdot \mathbf{B} dx = \int_{\Omega_0} \nabla \cdot \mathbf{B} dx \neq 0, \quad (18)$$

where  $\Omega_1$  corresponds to the volume between the surface  $S_1$  and the conductor and the  $\Omega_0$  to the volume of the cavity. The last equality follows since Maxwell's equations tell us that  $\nabla \cdot \mathbf{B} = 0$  in  $\Omega_1$  and  $\Omega_C$ . However, in the cavity,  $\Omega_0$ , we have notably not assumed this to be true since if  $\nabla \cdot \mathbf{B} = 0$  in  $\Omega_0$  there would be no need to consider a cavity. The case of  $\nabla \cdot \mathbf{B} \neq 0$  in  $\Omega_0$  corresponds to the presence of a magnetic monopole, which, incidentally, could also be modelled by this formulation.

In the case of  $\mathbf{A}$  based formulation, the surface integral becomes

$$\int_{S_1} \mathbf{n} \cdot \mathbf{B} ds = \int_{\Omega_1 + \Omega_C + \Omega_0} \nabla \cdot \text{curl } \mathbf{A} dx = 0, \quad (19)$$

and consequently, the  $\mathbf{A}$  based formulation, when unmodified, cannot be used to model a magnetic monopole. This is also what the theory predicts: since  $\beta_2(\Omega_C) = 1$  there exists a finite dimensional cohomology space  $\mathcal{H}^2(\Omega_C) \subset H(\text{div}, \Omega_C)$  of dimension  $\dim \mathcal{H}^2(\Omega_C) = \beta_2(\Omega_C) = 1$  and it is precisely this which represents the divergence free fields that are not the curl of some vector field. However, as the situations in which one might wish to model a magnetic monopole are rare we shall not pursue it further.

## 4 Which approach to follow

In the previous section we have illustrated two possible situations where eddy current problems contain a multiply connected domain. We observed that for the case of a conductor with a handle, the  $\mathbf{H}$  based formulation, with the choice of  $\mathbf{H}' = -\nabla\psi'$  in  $\Omega_N$ , required the insertion of cut in order to correct the fields although the  $\mathbf{A}$  based formulation did not. In the case of the conductor with a cavity, the  $\mathbf{H}$  based formulation is able to correctly predict the fields, although the  $\mathbf{A}$  based is not. However, as the case of a conductor with a handle is of greater practical relevance this shall be our focus.

For multiply connected domains with handles, one might be tempted to think that the  $\mathbf{A}$  based formulation is superior as it does not require the insertion of a cut into the computational domain. Nevertheless, there are other computational related drawbacks associated with the standard  $\mathbf{A}$  based formulation: Firstly, in the non-conducting region this formulation requires discretization of a vector field rather than a scalar field, which may lead to a greater number unknowns as there are generally a larger number of edges in tetrahedral meshes than vertices. Secondly, a conforming discretization of the  $\mathbf{A}$  based formulation (without gauging in  $\Omega_N$ ) results in singular linear system. This system may be solved iteratively provided that the right hand side is consistent [61]. If one applies gauging in  $\Omega_N$  by regularization (as in (12)), the resulting linear system is ill conditioned due to the choice of a small regularization parameter. Hence, one needs parameter-robust solvers in order to achieve stable solutions. To overcome these difficulties a popular choice is the so called  $\mathbf{A},\Phi\text{-}\mathbf{A}$  (often also referred to as the  $\mathbf{A},V\text{-}\mathbf{A}$  formulation) in which the vector potential is used in  $\Omega_C$  and  $\Omega_N$  and a scalar potential is used in  $\Omega_C$  [62, 13, 15, 17], the incorporation of the Coulomb gauge for this formulation is discussed for example in [15]. However, the  $\mathbf{A},\Phi\text{-}\mathbf{A}$ , formulation needs the right treatment of cuts for the scalar potential  $\Phi$  and also leads to a coupled problem at first hand. A comparison of the iterative solution of the ungauged  $\mathbf{A}$  based and ungauged  $\mathbf{A},\Phi\text{-}\mathbf{A}$  formulations when BiCG iterative solver with incomplete Cholesky factorisation preconditioner have been presented in [38]. These results indicate that, for this choice of preconditioner, the latter formulation performed better and the former experienced problems at higher frequencies. Further computational comparison between gauged formulations can be found in [15, 17].

In this work we will follow the  $\mathbf{A}$  based formulation described by (7). In the remaining part of the work we present an accurate discretization of (8), which uses an efficient parameter-robust solution technique incorporating a special variants of gauging by regularization introduced in Section 2.4.1, and a new problem-adapted preconditioner. Thereby, we overcome the difficulties usually associated with this formulation.

## 5 Conforming discretization by $hp$ -finite elements

This section presents a brief review of the main concepts of  $hp$ -finite elements and reduced basis gauging as introduced in [65, 78], which will be the starting point for the construction of efficient preconditioners for the eddy current problem following in Section 6.

For the discretization we assume a conforming regular simplicial triangulation of  $\Omega$ , which we denote by  $\mathcal{T}_h$ . We refer to the set of its vertices by  $\mathcal{V}_h$ , to the set of the edges by  $\mathcal{E}_h$  and to the set of the faces by  $\mathcal{F}_h$ .



## 5.1 Tangential-continuous $hp$ -finite elements and explicit kernel splitting

An  $H(\text{curl})$ -conforming finite element discretization relies on tangential continuity between element interfaces. The construction of low-order tangential-continuous elements - the Nédélec elements - date back to the work of Nédélec [57, 58]. There are several construction variants of high order  $H(\text{curl})$ -conforming basis functions, eg Demkowicz *et al.* [27, 59], Ainsworth and Coyle [1, 2] and Bossavit [20]. An essential property in all these constructions is the exactness of the discrete de Rham sequence - the discrete version of (3):

$$\begin{array}{ccccccc} \mathbb{R} & \xrightarrow{id} & H^1(\Omega) & \xrightarrow{\nabla} & H(\text{curl}, \Omega) & \xrightarrow{\text{curl}} & H(\text{div}, \Omega) & \xrightarrow{\text{div}} & L_2(\Omega) \\ & & \cup & & \cup & & \cup & & \cup \\ \mathbb{R} & \xrightarrow{id} & W_{h,p+1} & \xrightarrow{\nabla} & V_{h,p} & \xrightarrow{\text{curl}} & Q_{h,p-1} & \xrightarrow{\text{div}} & S_{h,p-2} \end{array} \quad (20)$$

In view of building an efficient preconditioner for the eddy current problem we rely on the special construction principle of the  $H(\text{curl})$ -conforming space  $V_{h,p}$  as introduced in [65].

We start with an arbitrary low-order vertex, high-order edge-face-cell based splitting of the hierarchic scalar  $H^1$ -conforming finite element space

$$W_{h,p+1} := W_{h,1} \oplus \sum_{\text{edges } E \in \mathcal{E}_h} W_{p+1}^E \oplus \sum_{\text{faces } F \in \mathcal{F}_h} W_{p+1}^F \oplus \sum_{\text{cells } I \in \mathcal{T}_h} W_{p+1}^I \subset H^1(\Omega), \quad (21)$$

as is common in the  $hp$ -framework see eg [25, 66, 67]. Here, the low-order space,  $W_{h,1}$ , is the classical scalar finite element space of continuous, piecewise linear hat functions. Its hierarchic edge-, face-, cell-based enrichment (21) allows for arbitrary varying polynomial degrees on each edge, face, and cell. In the case of a uniform polynomial degree we obtain the space of polynomials of total degree  $p+1$ , i.e.  $W_{h,p+1}|_T := P^{p+1}(T)$  on each element  $T \in \mathcal{T}_h$ .

Exploiting the locality of the gradients of the high-order edge-, face- and cell-based basis functions it is possible to construct a low-order edge, high-order edge-face-cell based splitting of the  $H(\text{curl})$ -conforming finite element space, which takes the following form

$$V_{h,p} := V_h^{\mathcal{N}_0} \oplus \sum_{\text{edges } E \in \mathcal{E}_h} \nabla W_{p+1}^E \oplus \sum_{\text{faces } F \in \mathcal{F}_h} \nabla W_{p+1}^F \oplus \tilde{V}_p^F \oplus \sum_{\text{cells } I \in \mathcal{T}_h} \nabla W_{p+1}^I \oplus \tilde{V}_p^I. \quad (22)$$

This is a direct sum of the discrete subsets of  $H(\text{curl}, \Omega)$ . The low-order space  $V_h^{\mathcal{N}_0}$  correspond to the lowest-order Nédélec space as introduced in [58]. The sub-spaces denoted by a tilde are local, linearly independent, and conforming completions of the face-based and cell-based gradient spaces. They are chosen such that firstly, the desired approximation order for  $V_{h,p}$  is obtained and secondly, that the exactness property

$$V_{h,p} \cap \nabla H^1(\Omega) = \nabla W_{h,p+1}, \quad (23)$$

holds. Detailed construction principles of the space splitting (22), as well as a concrete set of appropriate basis functions for tetrahedral elements can be found in [65]. Its generalisation to other element types can be found in [78].

The principal point of the splitting (22) is the explicit representation of the high-order gradient fields, which, among other advantages, plays a major role in the construction of parameter-robust and powerful preconditioners as presented in [65, 78] and is further exploited in the following sections.

## 5.2 Reduced basis gauging in non-conducting domain $\Omega_N$

In the sequel, we further distinguish between the sub-meshes of the conducting and the non-conducting domains. We denote the sub-triangulations of  $\mathcal{T}_h$  corresponding to  $\Omega_N$  and  $\Omega_C$  by  $\mathcal{T}_h^N$  and  $\mathcal{T}_h^C$ , respectively. Moreover, we refer to edges, faces and cells in the conducting domain  $\Omega_C$  by equipping the set of vertices, edges and cells by the additional index  $C$ .

The special construction of the  $H(\text{curl})$ -conforming  $hp$ -discretization (22) easily allows to skip the explicit higher-order gradients corresponding to the interior of  $\Omega_N$ . We define the reduced basis

$$V_{h,p}^{\text{red}} := V_h^{\mathcal{N}_0} \oplus \sum_{E \in \mathcal{E}_h^C} \nabla W_{p+1}^E \oplus \sum_{F \in \mathcal{F}_h^C} \nabla W_{p+1}^F \oplus \sum_{F \in \mathcal{F}_h} \tilde{V}_p^F \oplus \sum_{I \in \mathcal{T}_h^C} \nabla W_{p+1}^I \oplus \sum_{I \in \mathcal{T}_h} \tilde{V}_p^I. \quad (24)$$

There holds

$$V_{h,p}^{\text{red}}|_{\Omega_N} \cap \nabla H_0^1(\Omega_N) = \nabla W_{h,1}|_{\Omega_N} \cap \nabla H_0^1(\Omega_N) \quad \text{with} \quad \nabla W_{h,1} \subset V_h^{\mathcal{N}_0}. \quad (25)$$

The Galerkin approximation of the ungauged weak formulation (8) on the reduced space reads: Find  $\mathbf{A} \in V_{h,p}^{\text{red}} \cap H_0(\text{curl}, \Omega)$  such that

$$(\mu_r^{-1} \text{curl } \mathbf{A}, \text{curl } \mathbf{v})_{\Omega} + (\kappa \mathbf{A}, \mathbf{v})_{\Omega_C} = (\mu_0 \mathbf{J}^s, \mathbf{v})_{\Omega_C} \quad \forall \mathbf{v} \in H_0(\text{curl}, \Omega), \quad (26)$$

where a special variant of gauging introduced in Section 2.4.1 for the continuous problem is imposed on the reduced finite element space. In order to ensure unique solvability of (26) we impose a gauging condition on the low-order gradients  $\nabla W_{h,1} \subset V_{\mathcal{N}_0}$  by adding a regularization term analogous to  $\int_{\Omega_N} \varepsilon \mathbf{A} \cdot \mathbf{v} dx$  for the low-order Nédélec space  $V_{\mathcal{N}_0}$  space only. For the purpose of a concise presentation, we recall the definition of the perturbed parameter

$$\tilde{\kappa} = \begin{cases} \varepsilon & \text{in } \Omega_N \\ \kappa & \text{in } \Omega_C \end{cases}.$$

## 5.3 Resulting equations

Following the approach outlined above, the resulting parametric dependent algebraic systems of equations is: Find  $x \in \mathbb{C}^M$  such that

$$Kx = b, \quad (27)$$

where  $K$  is a complex symmetric matrix. Below, we adopt two different presentations for  $K$ .

Firstly, we decompose the degrees of freedom (d.o.f.) into those associated with low-order Nédélec space (subscript  $\mathcal{N}_0$ ), the high-order edge functions (gradients, subscript  $E$ ), the high-order face functions (subscript  $F$ ) and the high-order cell functions (subscript  $I$ ). Following [65, 78] we have that

$$K = \left[ \begin{array}{cccc} A_{\mathcal{N}_0 \mathcal{N}_0} & 0 & A_{\mathcal{N}_0 F} & A_{\mathcal{N}_0 I} \\ 0 & 0 & 0 & 0 \\ A_{F \mathcal{N}_0} & 0 & A_{FF} & A_{FI} \\ A_{I \mathcal{N}_0} & 0 & A_{IF} & A_{II} \end{array} \right] + \left[ \begin{array}{cccc} M_{\mathcal{N}_0 \mathcal{N}_0}(\tilde{\kappa}) & M_{\mathcal{N}_0 E}(\kappa) & M_{\mathcal{N}_0 F}(\kappa) & M_{\mathcal{N}_0 I}(\kappa) \\ M_{E \mathcal{N}_0}(\kappa) & M_{EE}(\kappa) & M_{EF}(\kappa) & M_{EI}(\kappa) \\ M_{F \mathcal{N}_0}(\kappa) & M_{FE}(\kappa) & M_{FF}(\kappa) & M_{FI}(\kappa) \\ M_{I \mathcal{N}_0}(\kappa) & M_{IE}(\kappa) & M_{IF}(\kappa) & M_{II}(\kappa) \end{array} \right]. \quad (28)$$

This matrix is comprised of terms originating from the stiffness matrix entries  $A_{ij} = \int_{\Omega} \mu_r^{-1} \text{curl } \varphi_i \cdot \text{curl } \varphi_j \, dx$  and the mass matrix entries  $M_{ij}(\kappa) = \int_{\Omega} \kappa \varphi_i \cdot \varphi_j \, dx$ , where  $\varphi_i$  is a typical basis function.

The second decomposition proves useful for the introduction of our novel preconditioning technique. For this decomposition, we begin by decomposing the d.o.f.'s into those associated with the low-order Nédélec space ( $\mathcal{N}_0$ ), the high-order gradient functions (in  $\Omega_C$ , subscript  $g$ ) and the remaining non-gradients functions (in  $\Omega$ , subscript  $n$ ). By reordering the degrees of freedom, we can express  $K$  as

$$K = \left[ \begin{pmatrix} A_{\mathcal{N}_0\mathcal{N}_0} & 0 & A_{\mathcal{N}_0n} \\ 0 & 0 & 0 \\ A_{n\mathcal{N}_0} & 0 & A_{nn} \end{pmatrix} + \begin{pmatrix} M_{\mathcal{N}_0\mathcal{N}_0}(\tilde{\kappa}) & M_{\mathcal{N}_0g}(\kappa) & M_{\mathcal{N}_0n}(\kappa) \\ M_{g\mathcal{N}_0}(\kappa) & M_{gg}(\kappa) & M_{gn}(\kappa) \\ M_{n\mathcal{N}_0}(\kappa) & M_{ng}(\kappa) & M_{nn}(\kappa) \end{pmatrix} \right]. \quad (29)$$

Moreover, due to the special construction of the  $H(\text{curl})$ -conforming basis functions, we identify, using appropriate superscripts for  $E$ ,  $F$  and  $I$ , that

$$\begin{aligned} K_{gg} &= \begin{pmatrix} K_{gg}^{EE} & K_{gg}^{EF} & K_{gg}^{EI} \\ K_{gg}^{FE} & K_{gg}^{FF} & K_{gg}^{FI} \\ K_{gg}^{IE} & K_{gg}^{IF} & K_{gg}^{II} \end{pmatrix}, \\ K_{nn} &= \begin{pmatrix} K_{nn}^{FF} & K_{nn}^{FI} \\ K_{nn}^{IF} & K_{nn}^{II} \end{pmatrix}, \\ K_{gn} &= \begin{pmatrix} K_{gn}^{EF} & K_{gn}^{EI} \\ K_{gn}^{FF} & K_{gn}^{FI} \\ K_{gn}^{IF} & K_{gn}^{II} \end{pmatrix}, \end{aligned}$$

and note  $K_{ng} = (K_{gn})^T$ . The identification of gradients and non-gradients was presented and proved in previous works [65, 78] to obtain parameter-robustness of any block-type Jacobi preconditioner for an elliptic parameter-dependent curl-curl problem as soon as the low-order space is treated correctly (see [65, 9, 32]). In this work, we use this explicit identification once more in order to treat gradients and non-gradients separately in the construction of a preconditioner for eddy current problems.

## 6 Efficient preconditioning

The proposed iterative approach for solving (27) consists of applying a preconditioner and a suitable iterative solution technique. The complex nature of  $K$  means that certain iterative solution techniques are not guaranteed to converge. Notably this includes the conjugate gradient algorithm, which is only guaranteed to converge for real symmetric positive definite matrices. The complex nature of the matrix limits the choice of iterative solution technique to those which can cope with matrices with complex eigenvalues, of which Generalised Minimum Residual (GMRES) and variants of Biconjugate Gradients (BICG) algorithms are possible candidates. In particular, the stabilised version of the BICG algorithm is preferred to standard BICG in order to overcome the difficulties associated with the breakdown of the standard version [63]. Despite these methods being suitable for complex matrices they may be slow to converge for large practical problems without a suitable preconditioner  $C^{-1}$ . It is recalled that a good preconditioner is one that is cheap to compute and is such that  $P^{-1}K \approx \mathbb{I}$  where  $\mathbb{I}$  is the identity matrix [63].

Schöberl and Zaglmayr have presented a parameter robust block Jacobi preconditioner, which is applied to magnetostatic and eigenvalue problems in [65], and, additionally, to eddy current problems in [78]. Using the decomposition of the d.o.f.'s presented in (28) this preconditioner takes the form  $P^{-1} = C^{-1}$  with

$$C = \begin{pmatrix} K_{\mathcal{N}_0\mathcal{N}_0} & 0 & 0 & 0 \\ 0 & \tilde{K}_{EE}(|\kappa|) & 0 & 0 \\ 0 & 0 & \tilde{K}_{FF}(|\kappa|) & 0 \\ 0 & 0 & 0 & \tilde{K}_{II}(|\kappa|) \end{pmatrix} \quad (30)$$

where the tilde is used to indicate that the block itself is block diagonal, i.e. only the d.o.f.'s associated to a single entity, an edge, a face or a cell, is used. When this preconditioner is expressed in terms of the alternative decomposition of the d.o.f.'s (29) it becomes

$$C = \begin{pmatrix} K_{\mathcal{N}_0\mathcal{N}_0} & 0 & 0 \\ 0 & C_{nn} & C_{gn} \\ 0 & C_{ng} & C_{gg} \end{pmatrix}, \quad (31)$$

where the blocks associated with the high-order gradient basis functions reduce to scaled mass matrices

$$\begin{aligned} C_{gg} &= \text{block diag}(\tilde{K}_{gg}^{EE}(|\kappa|), \tilde{K}_{gg}^{FF}(|\kappa|), \tilde{K}_{gg}^{II}(|\kappa|)) \\ &= \text{block diag}(\tilde{M}_{gg}^{EE}(|\kappa|), \tilde{M}_{gg}^{FF}(|\kappa|), \tilde{M}_{gg}^{II}(|\kappa|)), \end{aligned}$$

and

$$C_{gn} = \begin{pmatrix} 0 & 0 \\ \tilde{K}_{gn}^{FF}(|\kappa|) & 0 \\ 0 & \tilde{K}_{gn}^{II}(|\kappa|) \end{pmatrix} = \begin{pmatrix} 0 & 0 \\ \tilde{M}_{gn}^{FF}(|\kappa|) & 0 \\ 0 & \tilde{M}_{gn}^{II}(|\kappa|) \end{pmatrix} = (C_{ng})^T,$$

while the non-gradient block is

$$\begin{aligned} C_{nn} &= \text{block diag}(\tilde{K}_{nn}^{FF}(|\kappa|), \tilde{K}_{nn}^{II}(|\kappa|)) \\ &= \text{block diag}(\tilde{A}_{nn}^{FF} + \tilde{M}_{nn}^{FF}(|\kappa|), \tilde{A}_{nn}^{II} + \tilde{M}_{nn}^{II}(|\kappa|)). \end{aligned}$$

In the above, the tilde again indicate that the blocks are block diagonal.

The numerical experiments included in this work show that a substantial improvement is obtained for eddy current problems by exploiting the fact that the blocks of the system matrix,  $K$ , which are associated with the high-order gradient basis functions, reduce to scaled mass matrices and adopting a revised preconditioner for the iterative solution of  $Kx = b$ . By adopting the decomposition (29), the revised preconditioner takes the form  $P^{-1} = D^{-1}$  with

$$D = \begin{pmatrix} K_{\mathcal{N}_0\mathcal{N}_0} & 0 & 0 \\ 0 & D_{gg} & 0 \\ 0 & 0 & D_{nn} \end{pmatrix}, \quad (32)$$

where

$$\begin{aligned} D_{gg} &= \text{block diag}(i\tilde{M}_{gg}^{EE}(|\kappa|), i\tilde{M}_{gg}^{FF}(|\kappa|), i\tilde{M}_{gg}^{II}(|\kappa|), \\ D_{nn} &= \text{block diag}(\tilde{A}_{nn}^{FF} + \tilde{M}_{nn}^{FF}(|\kappa|), \tilde{A}_{nn}^{II} + \tilde{M}_{nn}^{II}(|\kappa|)). \end{aligned}$$

For the gradient block this special scaling in the preconditioner implies  $D_{gg}^{-1}(\text{block diag}(\tilde{K}_{gg})) = \mathbb{I}$ . By expressing the preconditioner in this way the application of the inverse of the high-order blocks corresponds to the solution of a linear system with a positive definite matrix, which, for the gradient blocks, is then post multiplied by  $1/i = -i$ . As these blocks are positive definite the application of the inverse can be achieved approximately by using a standard iterative solver, such as conjugate gradients, or exactly by using a direct solver. The low order space plays a special role and therefore the application of  $K_{\mathcal{N}_0\mathcal{N}_0}^{-1}$  is achieved by using a (sparse) direct solver.

As  $p$  is increased the number of cell-based d.o.f.'s grows rapidly. In particular, for three-dimensional problems, they grow at the rate  $O(p^3)$ . The cell-based d.o.f.'s are independent between each element and consequently a substantial reduction in the size of the linear system can be achieved by performing static condensation. This approach is adopted during the finite element assembly process, for further details see eg [39, 66]. After static condensation, the condensed gradient blocks will no longer solely scaled by  $\kappa$ . Nevertheless, motivated by the concept presented above, we still apply the same scaling,  $i|\kappa|$ , to the former gradient-blocks in the preconditioner for the condensed system and, as will be documented by the numerical experiments in the following section, this still yields a substantially improved iterative solver.

In the next section we investigate the benefits of the new preconditioner for a simple model problem. This is followed by an application of the approach to a set of challenging three-dimensional benchmark problems, which include both simply connected and multiply connected geometries.

## 6.1 Application of preconditioners to a model problem

The performance of the proposed iterative technique is first explored for a model problem in two-dimensions. The model problem relates to the solution of

$$\text{curl } \mu_r^{-1} \text{curl } \mathbf{A} + \kappa \mathbf{A} = \mu_0 \mathbf{J} \quad \text{in } \Omega, \quad (33a)$$

$$\mathbf{n} \times \mathbf{A} = 0 \quad \text{on } \partial\Omega, \quad (33b)$$

where the domain,  $\Omega$ , consists of two conducting cylinders, each of radius  $2 \times 10^{-3}m$ , separated by  $4.1 \times 10^{-3}m$  and surrounded by a non-conducting medium. The conductivity of the cylinders is initially set as  $\sigma = 10^4 S/m$ , the angular frequency is set as  $\omega = 100\pi$  and the relative permeability is set to one,  $\mu_r = 1$ . For this problem, our interest lies in the ability to efficiently solve the linear system rather than the actual solution of the problem. As the choice of right hand side does not influence the performance of the iterative solution technique, Dirichlet boundary conditions on  $\partial\Omega$  and the vector  $\mathbf{J}$  were arbitrarily set. The setup of the model problem is shown in Figure 4. The regularization parameter in the non-conducting region was set as  $\varepsilon = 10^{-5}$ , which is approximately 11 orders of magnitude smaller than  $\kappa$  in the conducting region.

To test the preconditioners proposed in Section 6, an unstructured mesh of 492 triangular elements is employed and uniform polynomial degrees  $p = 1, 2, 3, 4$  considered in turn. For each discretization, the eigenspectrum of the preconditioned linear system  $P^{-1}K$  using the matrices  $P = C$  and  $P = D$  is investigated. The eigenspectra of the preconditioned system matrices are shown in Figure 5. From this figure we can see a clear difference in the eigenspectra of the preconditioned systems. For the choice  $P = C$  we observe that, for all polynomial degrees considered, the eigenspectrum exhibits a wide degree of scattering of the points and

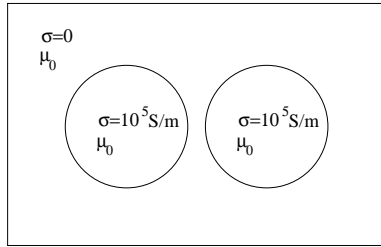


Figure 4: Illustration of a two-dimensional model problem used for the testing of the preconditioner

there is no clear pattern to the spectrum. On the other hand, the choice of  $P = D$  yields an eigenspectrum that exhibits a strong clustering about a point which is bounded away from zero. For both preconditioners, the changes in the eigenspectra of the preconditioned systems are small for increased  $p$ .

Given the strong clustering of the eigenvalues exhibited by the preconditioner  $P = D$  we expect this preconditioner to converge faster than preconditioner  $P = C$ . The number of iterations required for BICG (stabilised) and GMRES to reach a relative residual of  $10^{-5}$  is now investigated for the two preconditioning strategies and the different discretization. The results of this investigation are shown in Figure 6. From this figure we can observe that the number of iterations required to reach convergence using the preconditioner  $P = D$  is always less than when the preconditioner  $P = C$  is employed. The preconditioner  $P = D$  requires around 40% less iterations than  $P = C$  for this example. Comparing the BICG (stabilised) and GMRES iterative approaches, we observe that the convergence of GMRES is far smoother than that of BICG, the former exhibiting a linear convergence with almost every iteration leading to a reduction in the relative residual and the latter exhibiting somewhat more erratic convergence, although, in the majority of iterations, the relative residual is still reduced. Furthermore, we observe that the number of iterations is larger for BICG than GMRES, for the same choice of preconditioner. But, this does not necessarily mean that GMRES requires less computational effort than BICG. A single iteration of BICG requires two matrix products while GMRES requires only one, however, the cost of the GMRES iteration increases (in terms of floating point operations) as the iteration progresses [40]. To prevent the iterations of GMRES from becoming too expensive, a restart is performed every 5 (inner) iterations, which also limits the number of previous solution vectors that are required to be stored. If more solution vectors are stored a further reduction in the number of iterations would be obtained, although this would be at the expense of greater storage requirements.

As previously remarked, the choice of basis functions implies that the preconditioners are robust in  $\tilde{\kappa}$  [65]. This is also borne out in numerical experiments, Figure 7 shows the iterations obtained when the GMRES iterative solution algorithm was applied to the iterative solution of  $Kx = b$  and preconditioners  $P = C$  and  $P = D$  are applied to problems where the regularization parameter was fixed at  $\varepsilon = 10^{-5}$  and  $\sigma$  in the conducting regions was chosen as  $10^4, 10^5, 10^5, 10^7 S/m$  in turn. In Figure 7 we observe how the number of iteration remains robust with respect to varying  $\tilde{\kappa}$  for both the preconditioner  $P = C$  and the preconditioner  $P = D$ .

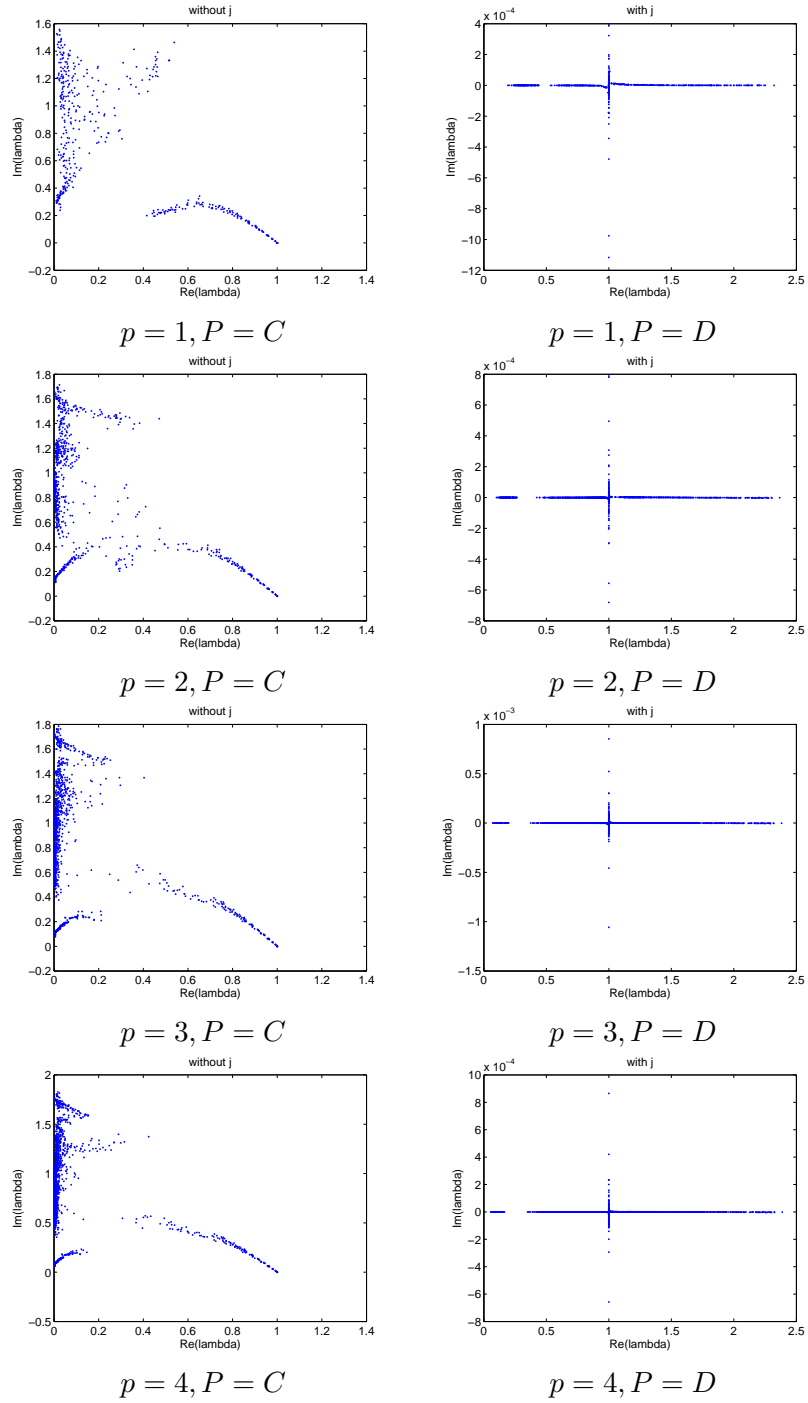


Figure 5: Two-dimensional model eddy current problem (33): The eigenspectra of  $P^{-1}K$  for the preconditioners  $P = C$  and  $P = D$ , a mesh of 492 unstructured triangular elements and the polynomial degrees  $p = 1, 2, 3, 4$

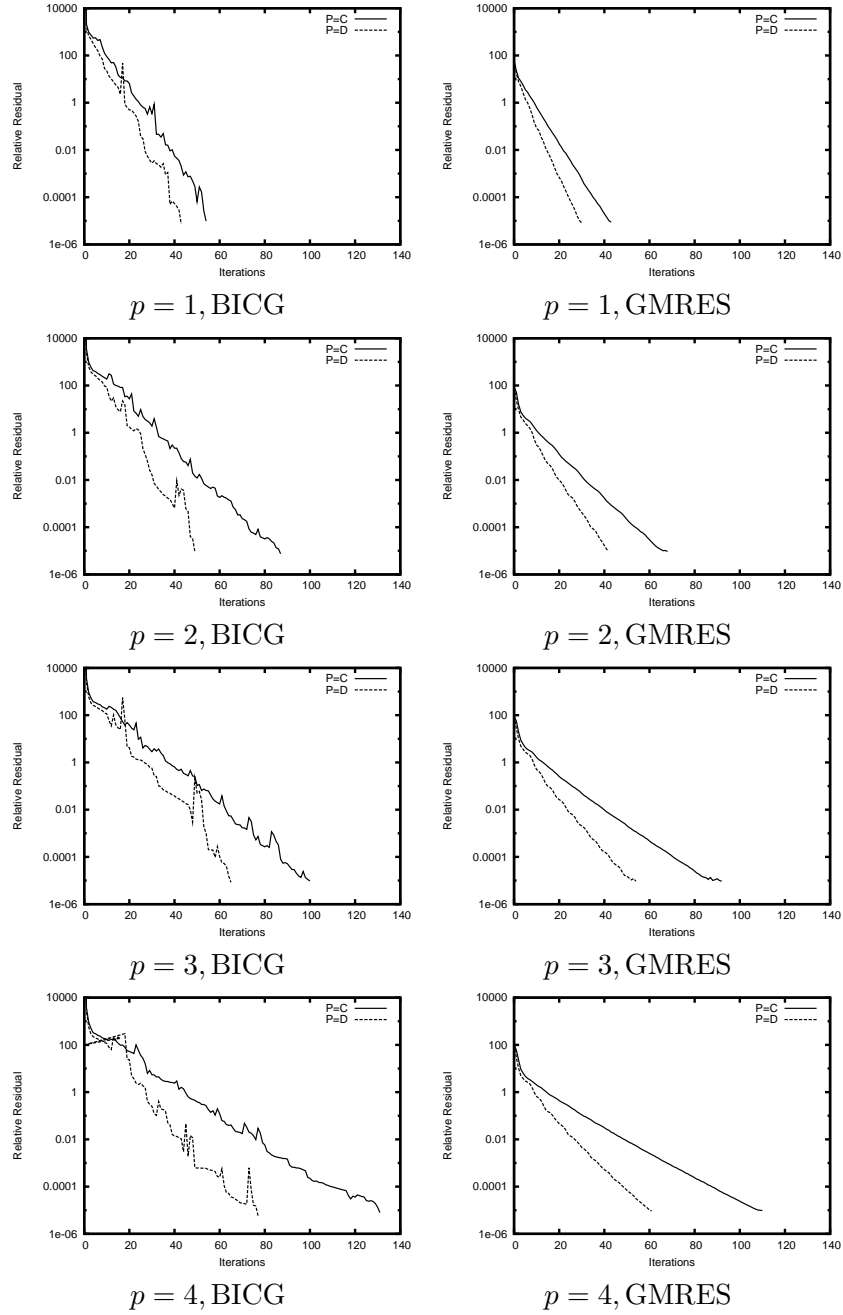


Figure 6: Two-dimensional model eddy current problem (33): The convergence of the iterative solvers BICG and GMRES for the preconditioners  $P = C$  and  $P = D$ , a mesh of 492 unstructured triangular elements and the polynomial degrees  $p = 1, 2, 3, 4$



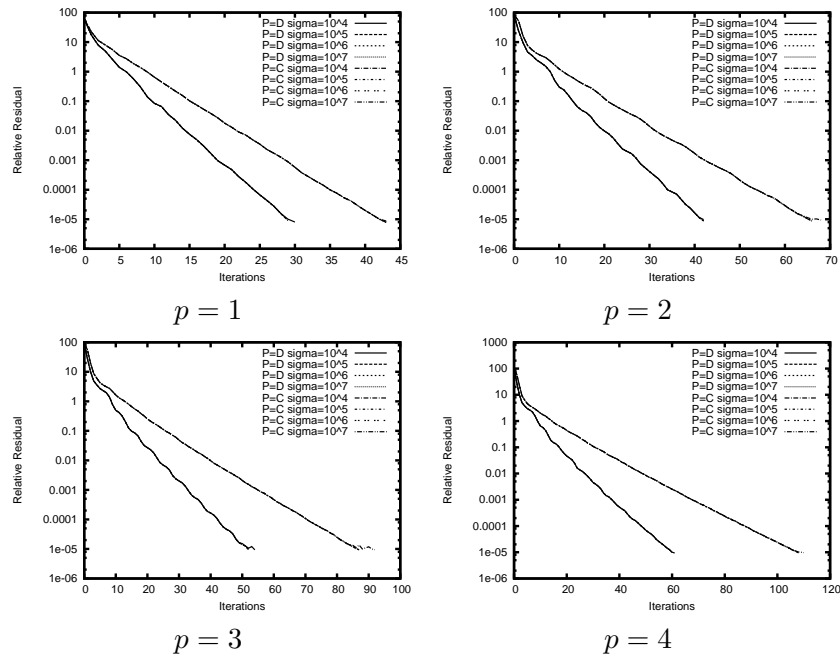


Figure 7: Two-dimensional model eddy current problem (33): The convergence of the iterative solvers GMRES for the preconditioners  $P = C$  and  $P = D$ , for varying  $\sigma$ , a mesh of 492 unstructured triangular elements and the polynomial degrees  $p = 1, 2, 3, 4$

## 7 Benchmark problems

The preconditioner  $P = D$  was seen to be clearly beneficial over  $P = C$  for the previous two-dimensional model problem. The effectiveness of the preconditioner will be now be demonstrated for two three-dimensional benchmark problems. The benchmark problems considered have been chosen from the set of problems proposed as part of series of COMPUMAG workshops. The problems are known as the TEAM (Testing of Electromagnetic Analysis Methods) benchmark problems [70] and are well established for testing computational electromagnetics software. Specifically, the benchmark problems 6 and 7 will be considered. The benchmark problem 6 consists of a conducting sphere in a uniform magnetic field for which an analytical solution is available (eg [56]). Numerical results for this benchmark problem have been reported using a variety of methods (eg [56, 69]). The second, and more challenging problem, consists of a conducting plate with a handle. This problem has no analytical solution, although experimental results [29] as well as other computational data [29, 38, 79] are available for making comparisons.

### 7.1 Conducting sphere in a uniform magnetic field

The TEAM benchmark problem 6 consists of a conducting sphere in a uniform magnetic field. The sphere has radius  $0.05m$  and material properties  $\mu_r = 20$  and  $\sigma = 10^7 Sm^{-1}$ . The surrounding free space has  $\mu_r = 1$  and  $\sigma = 0$ . The magnetic flux density is  $\mathbf{B} = (0, 0, 1)^T$  and the angular frequency is  $\omega = 100\pi rads^{-1}$ . This geometry represents a simply connected region.

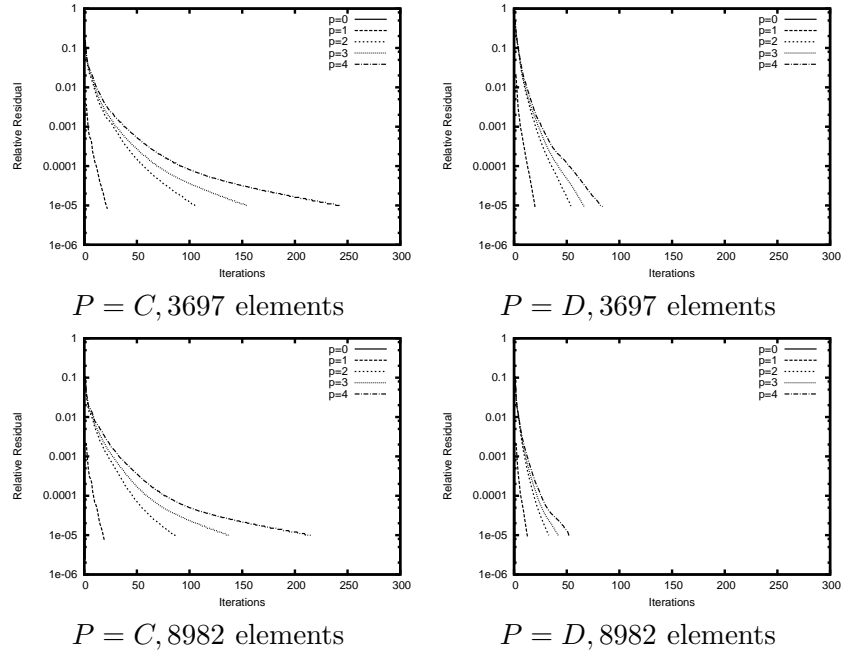


Figure 8: Conducting sphere in a uniform magnetic field: The convergence of GMRES using the preconditioners  $P = C$  and  $P = D$ , for the meshes of 3697 and 8982 tetrahedral elements and the polynomial degrees  $p = 0, 1, 2, 3, 4$

For the simulations, the computational domain was truncated with rectangular outer box on which  $\mathbf{n} \times \mathbf{A}$  was specified. The regions between the sphere and the outer box as well as inside the sphere were triangulated by unstructured meshes of tetrahedral elements using the FLITE mesh generator [72]. Using the mesh generator a coarse mesh of 3697 elements as well as a finer mesh of 8982 elements were generated. The regularization parameter for this example was set as  $\varepsilon = 10^{-6}$  in the non-conducting region, which is approximately 9 orders of magnitude smaller than  $\kappa$  in the conducting region. On each mesh elements of uniform polynomial degrees  $p = 0, 1, 2, 3, 4$  were considered. The performance of the preconditioners  $P = C$  and  $P = D$  for the iterative solution of the linear system using the GMRES algorithm, for each of the described discretizations, is shown in Figure 8.

Just as in the two dimensional model problem, we see that the choice of preconditioner  $P = D$  is far superior to using  $P = C$ . In this case, for both meshes, the preconditioner  $P = D$  needs only approximately 50% of the iterations required by  $P = C$  to reach the relative tolerance of  $10^{-5}$ .

The approximation of the geometry is undertaken separately to the field. If the linear geometry from the mesh generator is used, the surface of the sphere is poorly represented for the coarse meshes considered. The poor representation of the surface of the sphere limits the accuracy of the finite element approach when  $p$  refinement is performed. To overcome this, the approach previously described by Coyle and Ledger [23] is adopted to obtain an accurate description of the geometry. This approach involves the correction of the linear geometry along edges and faces. The degree of correction is expressed in terms of  $g$  where  $g + 1$  implies the polynomial degree of the geometry approximation. A suitable error measure

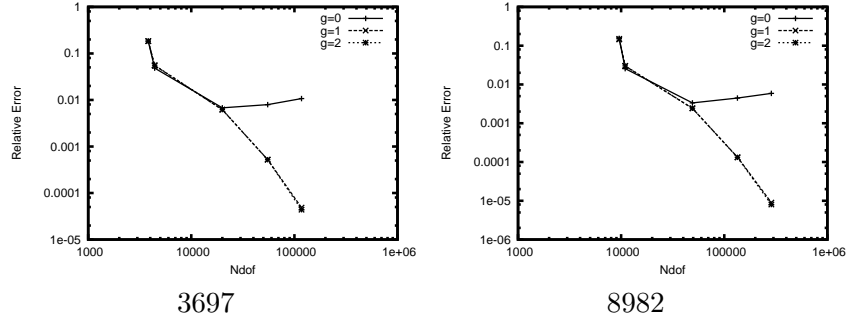


Figure 9: Conducting sphere in a uniform magnetic field: The convergence of  $\|\mathbf{J}^e - \mathbf{J}_H^e\|_{L_2(\partial\Omega_c)}^2$  against numbers of degrees of freedom, for meshes of 3697 and 8982 tetrahedral elements, the polynomial degrees  $p = 0, 1, 2, 3, 4$  and different orders of geometry correction

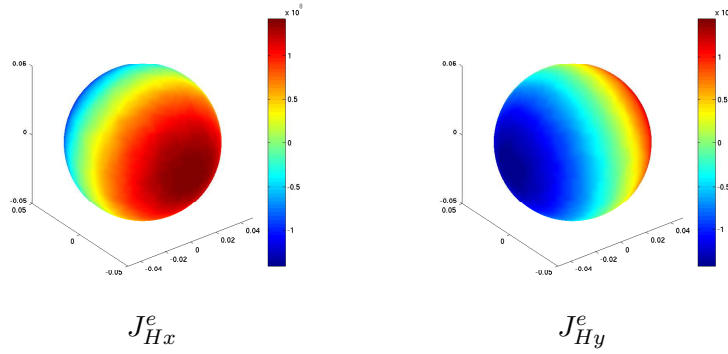


Figure 10: Conducting sphere in a uniform magnetic field: The distribution of the eddy current on the surface of the sphere  $\mathbf{J}_H^e = (J_{Hx}^e, J_{Hy}^e, 0)$  computed using the mesh of 3697 tetrahedra and  $p = 4$ .

for measuring the approximation of the eddy current is the  $L_2$  type norm

$$\|\mathbf{J}^e - \mathbf{J}_H^e\|_{L_2(\partial\Omega_c)}^2 = \int_{\partial\Omega_c} |\mathbf{J}^e - \mathbf{J}_H^e|^2 ds. \quad (34)$$

The computed eddy current is obtained from  $\mathbf{J}_H^e = -i\sigma\mathbf{A}_H$  and the analytical eddy current from the formulae in [56]. The error measure is computed for the meshes of 3697 and 8982 tetrahedral elements and uniform polynomial degrees  $p = 0, 1, 2, 3, 4$  in turn when the order geometry correction are  $g = 0, 1, 2$ . The results of this investigation are shown in Figure 9. The different curves indicate different orders of geometry correction and the points along the curve represent increasing polynomial degree. When the degree of correction is  $g = 0$  the geometry is not corrected and we observe that the error obtained by performing  $p$  refinement stagnate for both meshes at around 1%. However, for  $g = 1$  and  $g = 2$  performing  $p$  refinement leads to a rapid reduction in  $\|\mathbf{J}^e - \mathbf{J}_H^e\|_{L_2(\partial\Omega_c)}^2$ , which does not stagnate for the polynomial degrees considered. The downward shaping curve indicates that the convergence is exponential.

Contours of the computed solution for the eddy current on the surface of the sphere when the mesh of 3697 elements and  $p = 4$  elements are used are shown in Figure 10. These contours compare well with the contours of the eddy current distribution computed using the

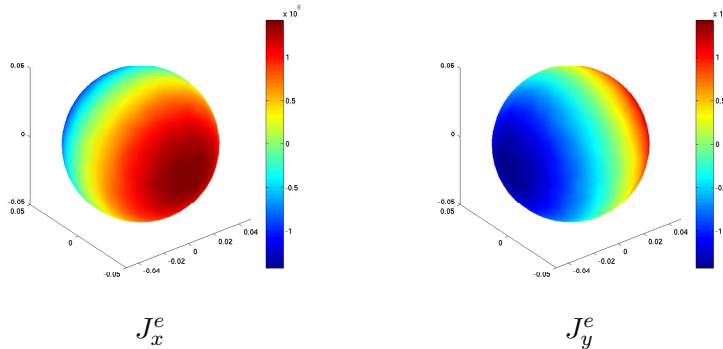


Figure 11: Conducting sphere in a uniform magnetic field: The distribution of the eddy current on the surface of the sphere  $\mathbf{J}^e = (J_x^e, J_y^e, 0)$  obtained from the analytical solution

analytical solution [56] shown in Figure 11. The contours of the eddy currents obtained using the mesh of 8982 tetrahedra and  $p = 4$  elements was also similar.

## 7.2 Asymmetrical conducting plate with a handle

The team benchmark problem 7 consists of a conducting plate with a handle <sup>4</sup>, which is placed eccentrically, is set asymmetrically in a non-uniform magnetic field [29]. The field is produced by a coil whose current varies sinusoidal with time. The dimensions of the problem can already be found in several sources [29, 38, 79] and therefore are not reproduced here. The conductivity of the plate is  $3.256 \times 10^7 Sm^{-1}$ , the maximum Ampere turn of the coil is 2742 and the frequencies operation are  $100\pi rad s^{-1}$  and  $400\pi rad s^{-1}$ . The relative permeability is  $\mu_r = 1$  everywhere. The benchmark problem represents a multiply connected domain, due to the presence of a *loop* passing through the plate. For computational purposes, the domain is truncated at a finite distance from the conducting plate where the boundary condition  $\mathbf{n} \times \mathbf{A} = 0$  is applied. A mesh of 7308 unstructured tetrahedral elements was then generated using the NETGEN mesh generator. Figure 12 shows a screen shot of the various components involved in the simulation as entered using the NETGEN open-source mesh generator [64].

Numerical results are presented in Figures 13 and 14 for the convergence of the preconditioned iterative solution strategy using the preconditioners  $P = C$  and  $P = D$ . Figure 13 shows the convergence of GMRES for uniform polynomial degrees  $p = 0, 1, 2, 3, 4$  when the frequency of operation was set as  $\omega = 100\pi rad s^{-1}$ . The results presented in Figure 14 are for uniform polynomial degrees  $p = 0, 1, 2, 3, 4$  when the frequency operation was set as  $\omega = 400\pi rad s^{-1}$ . The regularization parameter was set to be  $\varepsilon = 10^{-4}$  in the non-conducting region, which means that it is approximately 8 orders of magnitude smaller than  $\kappa$  in the conducting region, for both frequencies of operation. The tolerance for the relative residual was set as  $10^{-8}$ .

From Figures 13 and 14 it is clear that the number of iterations required by preconditioner  $P = D$  to reach the required tolerance is substantially lower than that required by  $P = C$  for the same polynomial degree and frequency of operation. The increase in iterations for higher  $p$  observed when the preconditioner  $P = D$  is applied is also much smaller than when

<sup>4</sup>We recall from Section 3.1 that this example is often referred to as a “conducting plate with a hole” in the literature

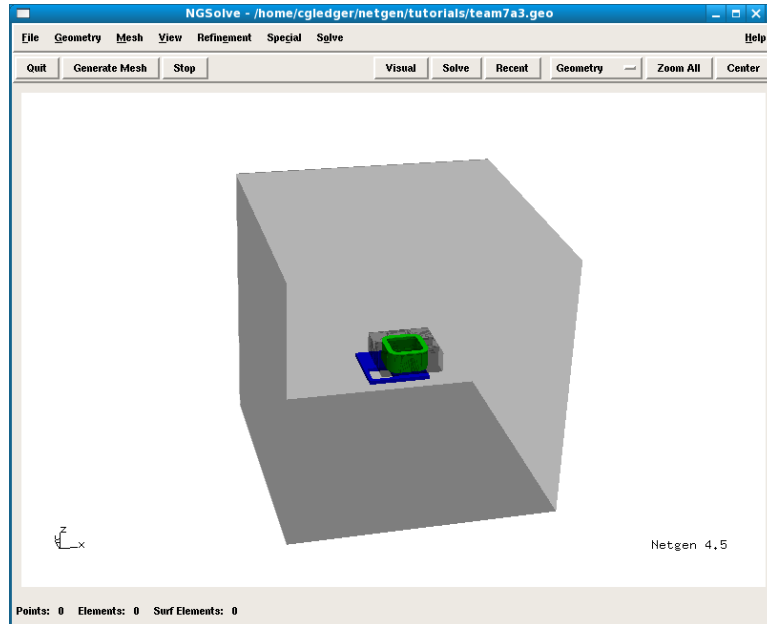


Figure 12: Illustration of a screen shot of the geometry for the TEAM benchmark problem 7 using the NETGEN software showing the coil in green and conducting plate with a handle in blue

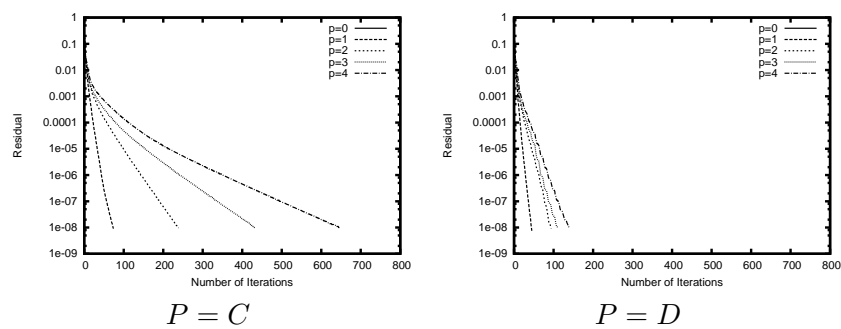


Figure 13: Conducting plate with a handle in a non-uniform magnetic field with  $\omega = 100\pi \text{rad s}^{-1}$ : The convergence of GMRES using the preconditioners  $P = C$  and  $P = D$ , for  $\varepsilon = 10^{-4}$ , a mesh of 7308 tetrahedral elements and the polynomial degrees  $p = 0, 1, 2, 3, 4$

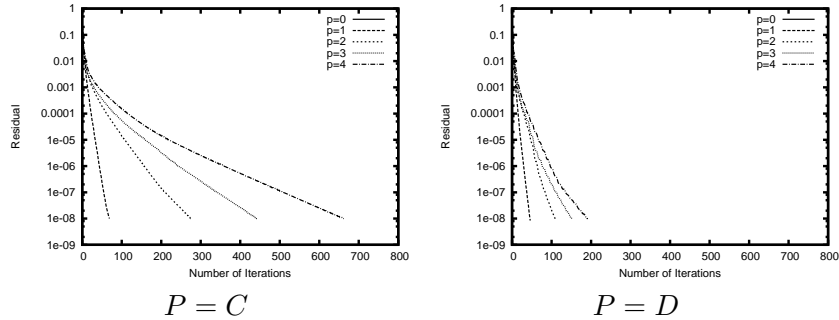


Figure 14: Conducting plate with a handle in a non-uniform magnetic field with  $\omega = 400\pi\text{rad s}^{-1}$ : The convergence of GMRES using the preconditioners  $P = C$  and  $P = D$ , for  $\varepsilon = 10^{-4}$ , a mesh of 7308 tetrahedral elements and the polynomial degrees  $p = 0, 1, 2, 3, 4$

the preconditioner  $P = C$  is applied. Although the preconditioners are robust in  $\tilde{\kappa}$ , a small variation in the number of iterations occurs for different values of  $\omega$  due to the rounding errors that accumulate when the iterations are performed.

To investigate the accuracy of the computations, the variation of the eddy current along an axis on the surface of the plate is plotted and compared against experimental results for both frequencies. Specifically, the quantity

$$\chi = \text{sign}\sqrt{\chi_R^2 + \chi_I^2}, \quad (35)$$

which was also used in [29], where  $\chi_R$  and  $\chi_I$  are the real and imaginary parts of a complex quantity and  $\text{sign} = \pm 1$  depending on whether  $\chi_R$  is positive or negative, is computed for the  $y$  components of eddy current,  $J_y^e$ , along the line  $y = 72 \times 10^{-3}m$ ,  $z = 19 \times 10^{-3}m$ .

The results of this investigation for  $\omega = 100\pi\text{rad s}^{-1}$  and  $\omega = 400\pi\text{rad s}^{-1}$  are shown in Figure 15. For both frequencies we first observe that increasing  $p$  leads to rapid convergence of the eddy current  $J_y^e$ . Secondly, for both frequencies, when  $p \geq 3$  the agreement between the computed solutions and the experimental results is excellent.

The computed contours of  $\mathbf{J}^e$  for  $\omega = 100\pi\text{rad s}^{-1}$  on the surface of the conducting plate for  $p = 4$  elements is shown in in Figure 16. The corresponding contours for  $\omega = 400\pi\text{rad s}^{-1}$  are shown in Figure 17.

## 8 Conclusions

In the first part of the work, we have presented a brief review of different formulations for solving the eddy current problem on multiply connected domains and through the presentation of two concrete examples highlighted the importance of using the correct mathematical treatment, which is available in the literature, eg [36, 19, 31] and references therein.

In the second part, we presented an accurate, efficient solution procedure for the  $\mathbf{A}$  based formulation of the eddy current problem on multiply connected domains with handles. We utilised a  $hp$ -finite element discretization and presented an improved block Jacobi preconditioner, which treats gradient blocks in a more natural way, as a novel contribution. The preconditioned system exhibited an eigenspectrum that is clustered and bounded away from

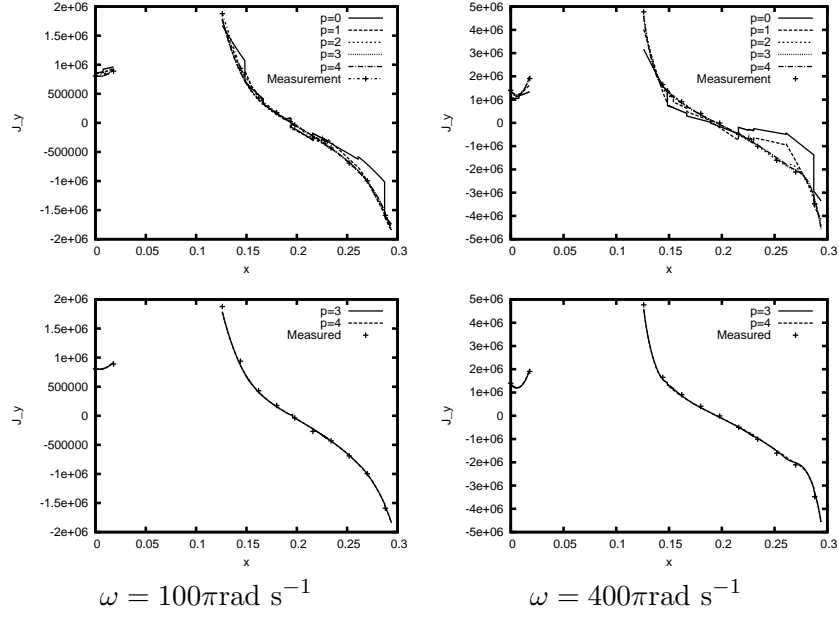


Figure 15: Conducting plate with a handle in a non-uniform magnetic field: The convergence of  $J_y$  on the line  $y = 72 \times 10^{-3}m$ ,  $z = 19 \times 10^{-3}m$  for increasing  $p$  and a comparison of the experimental and numerical values for  $J_y$ , when  $\omega = 100\pi\text{rad s}^{-1}$  and  $\omega = 400\pi\text{rad s}^{-1}$

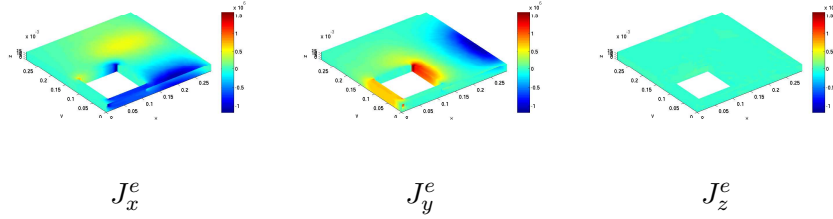


Figure 16: Conducting plate with a handle in a non-uniform magnetic field with  $\omega = 100\pi\text{rad s}^{-1}$ : The contours of  $\mathbf{J}^e$  on the surface of the conducting plate for uniform  $p = 4$  elements across a mesh of 7308 unstructured tetrahedral elements

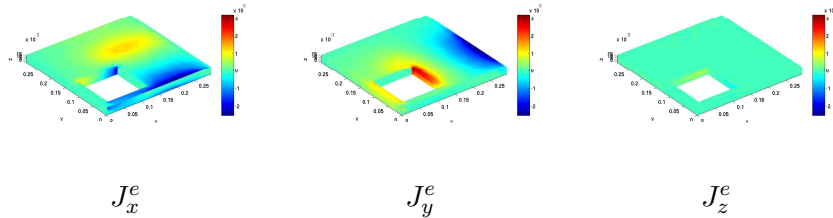


Figure 17: Conducting plate with a handle in a non-uniform magnetic field with  $\omega = 400\pi\text{rad s}^{-1}$ : The contours of  $\mathbf{J}^e$  on the surface of the conducting plate for uniform  $p = 4$  elements across a mesh of 7308 unstructured tetrahedral elements

0 in the complex plane, improving the efficiency of iterative solution techniques such as GMRES. Computational results showed that this led to a saving of between 40% – 75% in iterations for no additional computational effort. Furthermore, the use of  $hp$ -finite elements enabled accurate solutions to be computed that were in excellent agreement with analytical and experimental benchmark solutions.

For certain eddy current problems, in order to accurately resolve the small skin depth, one may prefer alternative discretizations, which might include the use of hybrid meshes and local mesh refinement. The  $H(\text{curl})$ -conforming basis proposed by Schöberl and Zaglmayr allows for such discretization and the preconditioner described in this work can be trivially extended to these.

## Acknowledgements

The authors gratefully acknowledge the support of the Royal Society Travel grant, the Austrian Science Foundation (FWF) through grant SFB/F32, and the University of Technology Graz, Austria, which enabled this joint research through the award of travel grants.

## References

- [1] M. Ainsworth and J. Coyle. Hierarchic  $hp$ -edge element families for Maxwell's equations on hybrid quadrilateral/triangular meshes. *Computer Methods in Applied Mechanics and Engineering*, 190:6709–6733, 2001.
- [2] M. Ainsworth and J. Coyle. Hierarchic finite element basis on unstructured tetrahedral meshes. *International Journal for Numerical Methods in Engineering*, 58:2103–2130, 2003.
- [3] M. Ainsworth, J. Coyle, P. D. Ledger, and K. Morgan. Computation of Maxwell eigenvalues using higher order edge elements. *IEEE Transactions on Magnetics*, 39:2149–2153, 2003.
- [4] M. Ainsworth and K. Pinchedez.  $hp$ -Approximation theory for BDRM/RT finite elements and applications. *SIAM Journal on Numerical Analysis*, 40:2047–2068, 2003.
- [5] H. Ammari, A. Buffa, and J. C. Nédélec. A justification of eddy current model for the maxwell equations. *SIAM Journal of Applied Mathematics*, 60(5):1805–1823, 2000.
- [6] D. N. Arnold, R. S. Falk, and R. Winther. Preconditioning in  $H(\text{div})$  and applications. *Mathematics of Computation*, 66(219):957–984, 1997.
- [7] D. N. Arnold, R. S. Falk, and R. Winther. Differential complexes and stability of finite element methods I: The de Rham complex. In D. Arnold, P. Bochev, R. Lehoucq, R. Nicolaides, and M. Shaskov, editors, *Compatible Spatial Discretizations*, volume 142 of *The IMA Volumes in Mathematics and its Applications*, pages 23–46. Springer, Berlin, 2006.
- [8] D. N. Arnold, R. S. Falk, and R. Winther. Finite element exterior calculus, homological techniques, and applications. *Acta Numerica*, 15:1–155, 2006.



- [9] D. N. Arnold and R. S. Falk and R. Winther. Multigrid in  $H(\text{div})$  and  $H(\text{curl})$ . *Numerische Mathematik*, 85(2):197–217, 2000.
- [10] F. Bachinger, U. Langer, and J. Schöberl. Numerical analysis of nonlinear multiharmonic eddy current problems. *Numerische Mathematik*, 100:594–616, 2005.
- [11] F. Bachinger, U. Langer, and J. Schöberl. Efficient solvers for nonlinear time-periodic eddy current problems. *Computing and Visualization in Science*, 9(4):197–207, December 2006. Springer.
- [12] R. Beck, P. Deuffhard, R. Hiptmair, R. H. W. Hoppe, and B. Wohlmuth. Adaptive multilevel methods for edge element discretizations of Maxwell’s equations. *Surveys on Mathematics for Industry*, 8(3–4):271–312, 1999.
- [13] O. Biro. Edge element formulations of eddy current problems. *Computer Methods in Applied Mechanics and Engineering*, pages 391–405, 1999.
- [14] O. Biro, P. Böhm, K. Preis, and G. Wachutka. Edge finite element analysis of transient skin effect problems. *IEEE Transactions on Magnetism*, 36:835–839, 2000.
- [15] O. Biro and K. Preis. On the use of the magnetic potential in the finite element of analysis of three dimensional eddy current problems. *IEEE Transactions on Magnetism*, 25:631–635, 1989.
- [16] O. Biro, K. Preis, and W. Renhart. Finite element analysis of 3D multiply connected eddy current problems. *IEEE Transactions on Magnetism*, 25:4009–4011, 1989.
- [17] O. Biro and A. Valli. The coulomb gauged vector potential formulation for the eddy current problem in general geometry: well-posedness and numerical approximation. Technical report, 2005. University of Trento - Italy - UNITN-Eprints (Italy).
- [18] A. Bossavit. Comments on magnetostatics with scalar potentials in multiply connected regions. *IEE Proceedings*, 136:260–261, 1989.
- [19] A. Bossavit. *Computational Electromagnetism*. Academic Press, 1998.
- [20] A. Bossavit. Generating Whitney forms of polynomial degree one and higher. *IEEE Transactions on Magnetism*, 38:341–344, 2002.
- [21] A. Bossavit and J–C Vériteé. A mixed FEM–BEM method to solve 3D eddy current problems. *IEEE Transactions on Magnetism*, 18:431–435, 1982.
- [22] W. Cecot, L. Demkowicz, and W. Rachowicz. A two dimensional infinite element for Maxwell’s equations. *Computer Methods in Applied Mechanics and Engineering*, 188:625–643, 2000.
- [23] J. Coyle and P. D. Ledger. Evidence of exponential convergence in the computation of Maxwell eigenvalues. *Computer Methods in Applied Mechanics and Engineering*, 194:587–604, 2004.
- [24] L. Demkowicz. *Computing with hp-Adaptive Finite Elements: Volume 1: One and Two Dimensional Elliptic and Maxwell Problems*. Chapman and Hall, 2007.

- [25] L. Demkowicz, J. Kurtz, D. Pardo, M. Paszynski, W. Rachowicz, and A. Zdunek. *Computing with hp-Adaptive Finite Elements: Volume 2:Frontiers: Three Dimensional Elliptic and Maxwell Problems with Applications*. Chapman and Hall, 2007.
- [26] L. Demkowicz and M. Pal. An infinite element for Maxwell’s equations. *Computer Methods in Applied Mechanics and Engineering*, 164:77–94, 1998.
- [27] L. Demkowicz and W. Rachowicz. A 2D *hp* adaptive finite element package for electromagnetics. Technical report, TICAM Report 98-15, University of Texas at Austin.
- [28] L. Demkowicz and L. Vardapetyan. Modeling of electromagnetic/scattering problems using *hp*-adaptive finite elements. *Computer Methods in Applied Mechanics and Engineering*, 152:103–124, 1998.
- [29] K. Fujiwara and T. Nakata. Results for benchmark problem 7 (assymmetrical conductor with a hole). *COMPEL - The International Journal for Computation and Mathematics in Electrical and Electronic Engineering*, 9:137–154, 1990.
- [30] V. Girault and P.-A. Raviart. *Finite element methods for Navier-Stokes equations: Theory and algorithms*. Springer, Berlin, 1986.
- [31] P. W. Gross and P. R. Kotiuga. *Electromagnetic Theory and Computation*. Cambridge University Press, 2004.
- [32] R. Hiptmair. Multigrid for Maxwell’s equations. *SIAM Journal of Numerical Analysis*, 36:204–225, 1999.
- [33] R. Hiptmair. Finite elements in computational electromagnetism. *Acta Numerica*, pages 237–339, 2002.
- [34] R. Hiptmair. Coupling of finite elements and boundary elements in electromagnetic scattering. *SIAM Journal of Numerical Analysis*, 41:621–640, 2003.
- [35] R. Hiptmair and P. D. Ledger. Computation of resonant modes for axisymmetric Maxwell cavities using *hp*-version edge finite elements. *International Journal for Numerical Methods in Engineering*, 62:1652–1676, 2005.
- [36] R. Hiptmair and O. Sterz. Current and voltage excitations for the eddy current model. *International Journal of Numerical Modelling, Electronic Networks, Devices and Fields*, 18:1–21, 2005.
- [37] A. Kameari. Three dimensional eddy current calculation using a finite element method with  $\mathbf{A} - V$  in conductor and  $\Omega$  in vacuum. *IEEE Transactions on Magnetics*, 24:118–121, 1988.
- [38] H. Kanayama, D. Tagami, K. Imoto, and S. Sugimoto. Finite element computation of magnetic field problems with the displacement current. *Journal of Computational and Applied Mathematics*, 159:77–83, 2003.
- [39] G. E. M. Karniadakis and S. Sherwin. *Spectral/hp Elements for Computational Dynamics*. Oxford Science Publications, Oxford, 2005.

- [40] C. T. Kelley. *Iterative Methods for Linear and Nonlinear Equations*. SIAM, 1995.
- [41] P. R. Kotigua. On making cuts for magnetic potentials in multiply connected regions. *Journal of Applied Physics*, 61:3916–3918, 1987.
- [42] P. R. Kotigua. Towards an algorithm to make cuts for magnetic scalar potentials in finite element meshes. *Journal of Applied Physics*, 63:3357–3359, 1987.
- [43] P. R. Kotigua. Comments on magnetostatics with scalar potentials in multiply connected regions. *IEE Proceedings*, 137:231–232, 1990.
- [44] M. Kuhn, U. Langer, and J. Schöberl. Scientific computing tools for 3D magnetic field problems. In John R. Whiteman, editor, *The Mathematics of Finite Elements and Applications X*, pages 239–258. Elsevier, 2000.
- [45] M. Kuhn and O. Steinbach. Symmetric coupling of finite and boundary elements for exterior magnetic field problems. *Mathematical Models in the Applied Sciences*, 25:357–371, 2002.
- [46] P. D. Ledger. *An hp-Adaptive Finite Element Procedure for Electromagnetic Scattering Problems*. PhD thesis, Dept. Civil Engineering, University of Wales, Swansea, 2002.
- [47] P. D. Ledger. An investigation of a preconditioner for high frequency Maxwell problems. *Electromagnetics*, 2009. accepted.
- [48] P. D. Ledger. Preconditioners for the indefinite linear system arising from the *hp* discretisation of Maxwell’s equations. *Communications in Numerical Methods in Engineering*, 25:275–289, 2009.
- [49] P. D. Ledger and K. Morgan. An adjoint enhanced reduced order model for monostatic RCS calculation in three–dimensions. *Electromagnetics*, 28:54–76, 2008.
- [50] P. D. Ledger, K. Morgan, and O. Hassan. Electromagnetic scattering simulation using an  $\mathbf{H}(\text{curl})$  conforming *hp* finite element method in three dimensions. *International Journal for Numerical Methods in Fluids*, 53:1267–1296, 2007.
- [51] P. D. Ledger, K. Morgan, O. Hassan, and N. P. Weatherill. Arbitrary order edge elements for electromagnetic scattering simulations using hybrid meshes and a PML. *International Journal for Numerical Methods in Engineering*, 55:339–358, 2002.
- [52] P. D. Ledger, J. Peraire, K. Morgan, O. Hassan, and N. P. Weatherill. Adaptive *hp* finite element computations of the scattering width output of Maxwell’s equations. *International Journal for Numerical Methods in Fluids*, 43:953–978, 2003.
- [53] P. D. Ledger, J. Peraire, K. Morgan, O. Hassan, and N. P. Weatherill. Parameterised electromagnetic scattering solutions for a range of incident wave angles. *Computer Methods in Applied Mechanics and Engineering*, 193:3587–3605, 2004.
- [54] P. Monk. *Finite Element Method for Maxwell’s Equations*. Oxford Science Publications, 2003.
- [55] T. Morisue. A new formulation of the magnetic vector potential method in 3D multiply connected regions. *IEEE Transactions on Magnetics*, 24:110–113, 1985.

- [56] T. Morisue and M. Fukumi. 3D eddy current calculation using the vector potential. *IEEE Transactions on Magnetics*, 24:106–109, 1988.
- [57] J. C. Nédélec. Computation of eddy currents on a surface in  $\mathbb{R}^3$  by finite element methods. *SIAM Journal of Numerical Analysis*, 15:580–594, 1978.
- [58] J. C. Nédélec. Mixed elements in  $\mathbb{R}^3$ . *Numerische Mathematik*, 35:315–341, 1980.
- [59] W. Rachowicz and L. Demkowicz. A three-dimensional *hp* adaptive finite element package for electromagnetics. *International Journal for Numerical Methods in Engineering*, 53:147–180, 2002.
- [60] S. Reitzinger and J. Schöberl. Algebraic multigrid for edge elements. *Numerical Linear Algebra with Applications*, 9:223–238, 2002.
- [61] Z. Ren. Influence on the rhs on the convergence behaviour of the curl-curl equation. *IEEE Transactions on Magnetics*, 32:655–658, 1996.
- [62] A. A. Rodriguez, P. Fernandes, and A. Valli. Weak and strong formulations for the time harmonic eddy-current problem in general multi-connected domains. *European Journal of Applied Mathematics*, 14:387–406, 2003.
- [63] Y. Saad. *Iterative Methods for Sparse Linear Systems*. SIAM, 2004.
- [64] J. Schöberl. NETGEN - An advancing front 2D/3D-mesh generator based on abstract rules. *Computing and Visualization in Science*, 1:41–52, 1997. <http://sourceforge.net/projects/netgen-mesher/>.
- [65] J. Schöberl and S. Zaglmayr. High order Nédélec elements with local complete sequence properties. *International Journal for Computation and Mathematics in Electrical and Electronic Engineering (COMPEL)*, 24:374–384, 2005.
- [66] C. Schwab. **p*- and *hp*- Finite Element Methods: Theory and Applications in Solid and Fluid Mechanics*. Oxford University Press, 1998.
- [67] B. Szabo and I. M. Babuska. *Finite Element Analysis*. John Wiley and Sons, 1991.
- [68] B. Szabo, A. Duester, and E. Rank. The *p*-version of the finite element method. In E. Stein, R. de Borst, and T. J. Hughes, editors, *Encyclopedia of Computational Mechanics*. Wiley, 2004.
- [69] H. Tsuboi and T. Misaki. Three-dimensional analysis of eddy current distributions by the boundary element method using vector variables. *IEEE Transactions on Magnetics*, 23:3044–3046, 1987.
- [70] L. R. Turner, K. Davey, C. R. I. Emson, K. Miya, T. Nakata, and A. Nicolas. Problems and workshops for eddy current code comparison. *IEEE Transactions on Magnetics*, 24, 1998.
- [71] A. Vourdas and K. J. Binns. Magnetostatics with scalar potentials in multiply connected regions. *IEE Proceedings*, 136:49–54, 1989.

- [72] N. P. Weatherill and O. Hassan. Efficient three-dimensional Delauney triangulation with automatic point creation and imposed boundary conditions. *International Journal for Numerical Methods in Engineering*, 37:2005–2039, 1994.
- [73] J. P. Webb. Hierarchical vector basis functions of arbitrary order for triangular and vector tetrahedra. *IEEE Transactions on Antennas and Propagation*, 47:1244–1253, 1999.
- [74] J. P. Webb and B. Forghani. A single scalar potential method for 3D magnetostatics using edge elements. *IEEE Transactions on Magnetics*, 25:4126–4128, 1989.
- [75] J. P. Webb and B. Forghani. A scalar vector method for 3d eddy current problems using edge elements. *IEEE Transactions on Magnetics*, 26:2367–2369, 1990.
- [76] J. P. Webb and B. Forghani. Hierarchical scalar and vector tetrahedra. *IEEE Transactions on Magnetics*, 29:1495–1498, 1993.
- [77] J. P. Webb and B. Forghani. The low frequency performance of  $H - \phi$  and  $T - \phi$  methods using edge elements for 3D eddy current problems. *IEEE Transactions on Magnetics*, 29, 1993.
- [78] S. Zaglmayr. *High Order Finite Element Methods for Electromagnetic Field Computation*. PhD thesis, Institut für Numerische Mathematik, Johannes Kepler Universität Linz, Austria, 2006.
- [79] W. Zheng, Z. Chen, and L. Wang. An adaptive finite element method for the  $\mathbf{H} - \psi$  formulation of time dependent eddy current problems. *Numerische Mathematik*, 103:667–689, 2006.

## Erschienenene Preprints ab Nummer 2008/01

- 2008/01 P. Urthaler: Schnelle Auswertung von Volumenpotentialen in der Randelementmethode.
- 2008/02 O. Steinbach (ed.): Workshop on Numerical Simulation of the Maxwell Equations. Book of Abstracts.
- 2008/03 G. Of, O. Steinbach, P. Urthaler: Fast Evaluation of Newton Potentials in the Boundary Element Method.
- 2008/04 U. Langer, O. Steinbach, W. L. Wendland (eds.): 6th Workshop on Fast Boundary Element Methods in Industrial Applications, Book of Abstracts.
- 2008/05 D. Brunner, G. Of, M. Junge, O. Steinbach, L. Gaul: A Fast BE-FE Coupling Scheme for Partly Immersed Bodies
- 2009/03 G. Of, O. Steinbach: The All-Floating Boundary Element Tearing and Interconnecting Method.
- 2009/04 O. Steinbach: A note on the stable coupling of finite and boundary elements.
- 2009/05 O. Steinbach, M. Windisch: Stable boundary element domain decomposition methods for the Helmholtz equation.
- 2009/06 G. Of, W. L. Wendland, N. Zorii: On the Numerical Solution of Minimal Energy Problems.
- 2009/07 U. Langer, O. Steinbach, W. L. Wendland (eds.): 7th Workshop on Fast Boundary Element Methods in Industrial Applications, Book of Abstracts.
- 2009/08 H. Egger, M. Freiberger, M. Schlottbom: Analysis of Forward and Inverse Models in Fluorescence Optical Tomography.
- 2009/09 O. Steinbach, M. Windisch: Robust boundary element domain decomposition solvers in acoustics.
- 2009/10 M. Freiberger, H. Egger, H. Scharfetter: Nonlinear Inversion in Fluorescence Optical Tomography.
- 2009/11 H. Egger, M. Hanke, C. Schneider, J. Schöberl, S. Zaglmayr: Adjoint Sampling Methods for Electromagnetic Scattering.
- 2009/12 H. Egger, M. Schlottbom: Analysis and Regularization of Problems in Diffuse Optical Tomography.
- 2009/13 G. Of, T. X. Phan, O. Steinbach: An energy space finite element approach for elliptic Dirichlet boundary control problems.
- 2009/14 G. Of, O. Steinbach: Coupled FE/BE Formulations for the Fluid-Structure Interaction.
- 2010/01 G. Of, T. X. Phan, O. Steinbach: Boundary element methods for Dirichlet boundary control problems.